Quaternary Science Reviews 390 (2026) 110188

Contents lists available at ScienceDirect

Quaternary Science Reviews

journal homepage: www.elsevier.com/locate/quascirev

# Fingerprinting paleotsunami deposits using sedimentary biomarkers – A succinct review and case study from a paleotsunami record on the Sanriku coastline (Noda, Japan)

Piero Bellanova[a,*], Jana Decker[a,b], Yuichi Nishimura[c], Catherine Chagué[d,e], Tetsuya Shinozaki[f], Daisuke Sugawara[g], Klaus Reicherter[a], Jan Schwarzbauer[b]

[a] Institute of Neotectonics and Natural Hazards, RWTH Aachen University, Germany
[b] Institute of Organic Biogeochemistry in Geo-Systems, RWTH Aachen University, Germany
[c] Institute of Seismology and Volcanology, Hokkaido University, Japan
[d] UNSW Sydney, School of Biological, Earth and Environmental Sciences, Australia
[e] Environmental Hazards, Earth Sciences New Zealand, Christchurch, New Zealand
[f] Department of Civil and Environmental Engineering, Chuo University, Japan
[g] International Research Institute of Disaster Science, Tohoku University, Japan

ARTICLE INFO

Handling Editor: Dr P Rioual

*Keywords:*
Paleotsunami
Lipid biomarkers
Geochemical signatures

ABSTRACT

Organic geochemical indicators have proven suitable to identify and characterize deposits of recent tsunamis, such as the 2011 CE Tōhoku-oki event, providing insights into erosional and transport processes of marine and terrestrial sediment inland (inundation) and offshore (backwash). However, lipid biomarkers have rarely been applied to historic and paleotsunami archives. We review lipid biomarkers suitable for paleotsunami research and present a case study using a targeted multi-compound approach on a geoslicer core from the Maita River Valley at Noda (Iwate Prefecture, Japan). At this site four paleotsunami deposits have previously been documented. In the analyzed samples, we quantified homologous series (*n*-alkanes, *n*-aldehydes, fatty acids), isoprenoids (pristane, phytane), terpenoids, diagenetically stable compounds (steranes, hopanes), and evaluated diagnostic ratios.

All four paleotsunami sand layers show a coherent marine fingerprint relative to background sediment. This fingerprint is expressed by enrichment of short-chain homologues, $C_{27}$ steranes and reduced $C_{29}/C_{27}$ sterane ratios, low pristane/phytane (≤0.7) with aquatic-sources clustering in the pristane/*n*-$C_{17}$ vs phytane/*n*-$C_{18}$ cross-plot, and lower sterane/hopane ratios. Terrigenous inputs are suppressed (lower long-chain homologues and TAR indices), while elevated OEP, CPI, and EOP ratios indicate rapid burial of relatively fresh plant waxes co-transported during inundation.

These results demonstrate that lipid biomarkers preserve paleotsunami signatures for millennia and can refine source allocation, sediment transport pathways, and complement sedimentological approaches, by characterizing and reconstructing the inundation of paleotsunamis. Such multi-compound lipid biomarker approaches enable more robust paleotsunami detection and improve constraints for regional tsunami-hazard assessments.

## 1. Introduction

Paleotsunami research is an important cornerstone of coastal hazard assessment because it extends records of tsunamigenic events beyond the instrumental and historical periods. By identifying and characterizing event deposits preserved in Holocene strata, we can constrain recurrence intervals and the range of plausible magnitudes for past tsunamis. Over the last three decades, contemporary tsunamis, most notably the 2004 CE Indian Ocean and 2011 CE Tōhoku-oki events, have transformed the research field, refining our understanding of syn- and post-tsunami processes, including hydrodynamics, erosion, transport, deposition, and preservation (e.g., Goto et al., 2011, 2014; Jagodziński et al., 2012; Richmond et al., 2012). Parallel advances in the detection of telltale geochemical signatures have improved identification and

* Corresponding author.
*E-mail address:* p.bellanova@nug.rwth-aachen.de (P. Bellanova).

https://doi.org/10.1016/j.quascirev.2026.110188
Received 17 March 2026; Received in revised form 20 July 2026; Accepted 21 July 2026
Available online 26 July 2026

characterization of tsunami deposits in sedimentary records (e.g., Chagué-Goff et al., 2011, 2012; Shinozaki et al., 2015; Szczuciński et al., 2016; Bellanova et al., 2020, 2021). At the same time, advances in tsunami modeling (e.g., Sugawara, 2021) and improvements in hazard assessments and coastal defenses by learning from the underestimation of recent events (e.g., Goto et al., 2011; Bernard, 2012; Suppasri et al., 2016), have transformed our ability to reconstruct past tsunamis and significantly improved our understanding of tsunami hazards worldwide.

Since the 2011 Tōhoku-oki tsunami, a multitude of new approaches and methodological tools that complement sedimentological investigations have been developed, such as sediment ancient and environmental DNA investigations (e.g., Hiraoka et al., 2016; Szczuciński et al., 2016; Yap et al., 2021, 2023; Shinozaki et al., 2025) and organic marker analyses (e.g., Alpar et al., 2012; Mathes-Schmidt et al., 2013; Shinozaki et al., 2015; Bellanova et al., 2020). Investigations of organic geochemical compounds, both lipid biomarkers (e.g., Shinozaki et al., 2015, 2016, 2022; Bellanova et al., 2020, 2021; Konechnaya et al., 2022) and organic pollutants (e.g., Bellanova et al., 2020, 2021; Frenken et al., 2022a, 2022b) from 2011 Tōhoku-oki tsunami deposits were fruitful. Biomarkers have proven to be a comprehensive tool providing insights into transport processes based on the source specificity of individual lipid compounds (Alpar et al., 2012; Shinozaki et al., 2015, 2022; Bellanova et al., 2021), providing environmental (e.g., Frenken et al., 2022a; Bellanova et al., 2023) and pollution information (Mizukawa et al., 2017; Frenken et al., 2022b) on tsunami sediments, and allowing detection of '*invisible*' tsunami deposits beyond the sand limit (Bellanova et al., 2021; Shinozaki et al., 2022; Komeiji et al., 2025). They have helped refine inundation limits where sedimentological criteria are ambiguous (e.g., Shinozaki et al., 2015, 2022; Bellanova et al., 2020, 2021), thus constituting a promising approach for future tsunami research (e.g., Shinozaki et al., 2015; Bellanova et al., 2020). Nevertheless, organic geochemical markers have predominantly been applied to deposits of recent or contemporary tsunami sediments and have been used only rarely in studies of known historic or paleotsunami deposits (e.g., Alpar et al., 2012; Ünlü et al., 2012; Mathes-Schmidt et al., 2013; Bellanova et al., 2023; Komeiji et al., 2025). This study aims to compile a database of suitable lipid biomarkers for paleotsunami research, review their environmental information value and limitations, explore additional diagnostic lipid biomarker proxies and ratios, and provide a case study example of their application to paleotsunami deposits from the Maita River Valley in Noda (Iwate Prefecture, Japan).

## 2. Biomarker proxies for paleotsunamis: current state of knowledge

Traditionally, identification of paleotsunami deposits in coastal lowlands depends largely on the presence and distribution of sand sheets. While this approach has proven successful for identifying paleotsunami deposits in the past, it was also affected by shortcomings. These include the possibility that sand sheets do not represent the maximum inundation extent (e.g., Goto et al., 2011; Chagué-Goff et al., 2012; Sugawara et al., 2012), the reliance and limitation to visual recognition (e.g., Chagué-Goff et al., 2012, 2015; Judd et al., 2017; Bellanova et al., 2021), restricted insights into processes by a stand-alone proxy (e.g., Kortekaas and Dawson, 2007; Chagué-Goff, 2010; Chagué-Goff et al., 2017), and uncertainties related to the preservation, recovery potential and post-depositional changes of thin deposits (e.g., Spiske et al., 2013, 2020; Chagué-Goff et al., 2015, 2017). These limitations can lead to misconceptions about the magnitude of paleotsunami events and the subsequent underestimation of the hazard potential (Goto et al., 2011; Bernard, 2012; Sugawara et al., 2012). This is especially true for the Japanese coastline prior to the 2011 Tōhoku-oki tsunami, where the hazard assessment was based on the 869 CE Jōgan tsunami (e.g., Satake, 2008; Namegaya et al., 2010; Sugawara et al., 2012). While the 869 CE Jōgan and 2011 Tōhoku-oki tsunamis are comparable, they possess notable differences in their sediment distribution (Goto et al., 2011; Namegaya and Satake, 2014). This is partially a function of erodable/transportable sedimentary material available at source areas (e.g., nearshore offshore, beach, dunes, backshore). Studies after the 2011 Tōhoku-oki tsunami showed that mud associated with deposits commonly reached significantly farther inland than sand, implying earlier inundation limits for the Jōgan event were likely underestimated (Goto et al., 2011; Chagué-Goff et al., 2012; Sugawara et al., 2012; Namegaya and Satake, 2014).

These '*invisible*' muddy deposits, often visually indistinct from the underlying soil or peat, necessitate more sensitive proxies. This has driven the development of geochemical fingerprinting to identify allochthonous material, even in the absence of clear visual evidence (Chagué-Goff, 2010; Chagué-Goff et al., 2011). Among these, organic lipid biomarkers have emerged as a particularly powerful tool for tracing tsunami deposits in the sedimentary record (Shinozaki et al., 2015; Bellanova et al., 2020, 2021). Early studies pioneered the application of lipid biomarkers (e.g., Alpar et al., 2012; Ünlü et al., 2012; Mathes-Schmidt et al., 2013), however, the first comprehensive biomarker study on modern tsunami deposits by Shinozaki et al. (2015) influenced the establishment and advancement of this approach for tsunami research.

Initial geochemical approaches often rely on bulk proxies, such as total organic carbon (TOC) or loss-on-ignition (LOI), C/N ratios, and stable carbon ($\delta^{13}C$) and nitrogen ($\delta^{15}N$) isotopes. These are effective for distinguishing between bulk terrestrial ($C_3$ plant) and marine (phytoplankton) organic matter sources (e.g., Chagué-Goff et al., 2012; Pilarczyk et al., 2012; Shinozaki et al., 2016). However, molecular lipid biomarkers offer greater specificity. The most widely used organic compounds in tsunami research are homologous series such as *n*-alkanes, fatty acids, or *n*-aldehydes (Table 1). Long-chained homologues of *n*-alkanes ($C_{26}$–$C_{35}$), fatty acids ($C_{22:0}$–$C_{32:0}$), and *n*-aldehydes ($C_{24}$–$C_{32}$) are derived from terrestrial plant waxes (e.g., Eglinton and Hamilton, 1967; Meyers, 1997). In contrast, the short-chain homologue counterparts of *n*-alkanes ($C_{11}$–$C_{21}$), fatty acids ($C_{14:0}$–$C_{18:0}$), and *n*-aldehydes ($C_{16}$–$C_{22}$) are ubiquitous in the environment (algae, bacteria; e.g., Meyers and Ishiwatari, 1993; Volkman et al., 1998; Meyers, 2003) but are generally associated with input of marine organic matter (e.g., Meyers, 1997; Budge and Parrish, 1998). Ratios between these groups, such as the terrigenous-to-aquatic ratio for *n*-alkanes ($TAR_{ALK}$) or fatty acids ($TAR_{FA}$) (Table 1), serve as distinctive and quantitative indicators of allochthonous marine input by a tsunami in a terrestrial environment (Bellanova et al., 2020; Konechnaya et al., 2022). Occasionally, other diagnostic ratios of these homologous lipid biomarker classes have been used, including the odd-even predominance ($OEP_{ALK}$, $EOP_{ALD}$; Bellanova et al., 2020, 2023), carbon preference index ($CPI_{ALK}$; Bellanova et al., 2020, 2023), and aquatic plant proxy ($P_{aq}$; Gaffney et al., 2020).

Sterols are another group of lipid biomarkers applied across different tsunami studies (Alpar et al., 2012; Shinozaki et al., 2015; Konechnaya et al., 2022, Table 1). $C_{27}$ sterols (e.g., cholesterol) are characteristic of marine fauna (zooplankton), whereas $C_{28}$ sterols (e.g., brassicasterol) trace marine and aquatic phytoplankton (diatoms, haptophytes), and $C_{29}$ sterols (e.g., β-sitosterol, stigmasterol) are dominant in terrestrial higher plants (e.g., Volkman, 1986, 2003; Volkman et al., 1998). The $C_{29}/C_{27}$ sterol ratio is a robust proxy for marine vs. terrestrial input (Volkman, 1986). Other, more source-specific biomarkers have been successfully applied, such as sesquiterpenes (e.g., isolongifolene) used to trace organic matter from coastal pine forests (*Pinus thunbergii*) eroded by the 2011 Tōhoku-oki tsunami (Shinozaki et al., 2022). Biomarkers with marine source specificity, such as alkenones produced by coccolithophores (Komeiji et al., 2025) or marine sterols (e.g., dinosterol; Alpar et al., 2012; Shinozaki et al., 2015), have been applied with mixed results. Particularly, alkenones are rarely detected in tsunami deposits due to degradation or low concentrations (Shinozaki et al., 2015).

In contrast, steranes and hopanes, the diagenetic products of sterols

**Table 1**
Biomarker proxies used in tsunami research with typical sources/indications and example references.

| Class | Specific Compound | Source/Indication | Examples |
|---|---|---|---|
| ***n*-alkanes** | short-chain *n*-alkanes $C_{15}$, $C_{17}$, $C_{19}$ | ubiquitous in nature from algae and bacteria, general indicator for marine/freshwater aquatic matter input from marine and freshwater sources | Alpar et al. (2012) Ünlü et al. (2012) Shinozaki et al. (2015, 2022) Bellanova et al. (2021, 2023) Frenken et al. (2022a) Komeiji et al. (2025) |
| | long-chain *n*-alkanes $C_{27}$, $C_{29}$, $C_{31}$ | unambiguous indicator of land-derived organic matter, general indicator for epicuticular waxes of terrestrial higher plants | Alpar et al. (2012) Ünlü et al. (2012) Shinozaki et al. (2015, 2022) Bellanova et al. (2021, 2023) Frenken et al. (2022a) |
| | $TAR_{ALK}$ (terrigenous to aquatic ratio) | ratio of long-chain to short-chain *n*-alkanes quantifying terrestrial vs. aquatic input | Bellanova et al. (2020, 2023) Frenken et al. (2022a) |
| | $OEP_{ALK}$ (odd-even predominance) | the odd-over-even predominance of *n*-alkanes where high values indicate fresh higher-plant wax input and low values indicate microbial or degraded OM | Bellanova et al. (2020, 2023) |
| | $CPI_{ALK}$ (carbon preference index) | odd/even index for *n*-alkanes where high values indicate recent higher-plant waxes and low values mature or strongly reworked organic matter | Bellanova et al. (2020, 2023) |
| | aquatic plant proxy ($P_{aq}$) | calculated as $(nC_{23} + nC_{25})/(nC_{23} + nC_{25} + nC_{29} + nC_{31})$, high values indicate submerged/floating macrophyte input relative to emergent/terrestrial plants | Gaffney et al. (2020) |
| **isoprenoids** | pristane ($C_{19}H_{40}$), phytane ($C_{20}H_{42}$) | diagenetic products of phytoplanktonic chlorophyll indicating marine primary productivity | Alpar et al. (2012) Ünlü et al. (2012) Shinozaki et al. (2015) |
| | pristane/phytane ratio (pr/ph) | indicator of depositional redox conditions | Alpar et al. (2012) Bellanova et al. (2023) |
| | pr/*n*-$C_{17}$ vs. ph/*n*-$C_{18}$ ratio | diagnostic ratio indicating with low values fresh organic matter and with high values algal/bacterial organic matter and/or biodegradation | Bellanova et al. (2023) |
| **$C_{27}$-, $C_{28}$- and $C_{29}$-sterol homologues** | $C_{27}$ sterols (cholersterol) | indicator of marine faunal organic matter of zooplankton and marine invertebrates | Shinozaki et al. (2015) Konechnaya et al. (2022) |
| | $C_{28}$ sterols (brassicasterol) | Originating from microalgal (diatoms/haptophytes) sources, indicating marine phytoplankton organic matter | Alpar et al. (2012) Shinozaki et al. (2015) |
| | $C_{29}$ sterols/phytosterols (β-sitosterol, stigmasterol) | unambiguous indicator of terrestrial organic matter from higher land plants | Shinozaki et al. (2022) |
| | $C_{29}/C_{27}$ sterol ratio | ratio of terrestrial ($C_{29}$) to marine-associated ($C_{27}$) sterols | Konechnaya et al. (2022) |
| | other marine sterols (dinosterol) | dinosterol is an indicator of marine organic matter input from dinoflagellates | Alpar et al. (2012) Shinozaki et al. (2015) |
| **hopanes** | biohopanes $\sum C_{29}$-$C_{35}$ | immature biohopanes ($C_{29}$-$C_{35}$) are linked to a biological synthesis by bacteria or plants | Bellanova et al. (2023) |
| | TS/TM ratio | ratio of $C_{27}$ 18α (H)-trisnorneohopane (TS) to $C_{27}$ 17α (H)-trisnorhopane) (TM) is sensitive to the depositional environment and the organic matter source | Bellanova et al. (2023) |
| **steranes** | $C_{27}$ steranes | $C_{27}$ homologues indicate marine algae/zooplankton sources | Bellanova et al. (2023) |
| | $C_{28}$ steranes | $C_{28}$ homologues indicate algae and fungi often from lagoonal environments | Bellanova et al. (2023) |
| | $C_{29}$ steranes | $C_{29}$ homologues indicate higher-plant (terrestrial) inputs | Bellanova et al. (2023) |
| | S/H ratio (sterane/hopane) | diagnostic ratio indicating with higher S/H values eukaryotic contribution and with lower values bacterial input of organic matter | Bellanova et al. (2023) |
| **fatty acids** | short-chain fatty acids (SCFA $C_{11:0}$-$C_{18:0}$) | general indicator of aquatic organic matter from algae and bacteria | Alpar et al. (2012) Konechnaya et al. (2022) |
| | long-chain fatty acids (LCFA $C_{22:0}$-$C_{32:0}$) | indicator of land-derived organic matter originating from terrestrial plant waxes | Alpar et al. (2012) |
| | polyunsaturated fatty acids (PUFAs) | can be specific to certain algal groups and planktic organisms | Alpar et al. (2012) |
| | $C_{16:1}/C_{16:0}$ FA ratio | diatom/algal indicator with elevated values reflecting diatom-rich inputs (note: ratios often decrease during settling/early diagenesis) | Alpar et al. (2012) Ünlü et al. (2012) |
| | $\sum C_{16}/\sum C_{18}$ FA ratio | relative abundance of $C_{16}$ vs $C_{18}$ fatty acids reflects algal/diatom/bacterial inputs with high values and terrestrial/macrophyte inputs with low values | Alpar et al. (2012) |
| | marine fatty acids & ratios (22:5ω3/20:5ω3; 20:1 + 22:1; 18:2ω6 & 18:3ω3) | marine fatty acids and ratios reflect plankton (zooplankton) and is useful to contrast marine (green algae) to terrestrial-macrophyte inputs | Alpar et al. (2012) Ünlü et al. (2012) |

(*continued on next page*)

**Table 1** (*continued*)

| Class | Specific Compound | Source/Indication | Examples |
|---|---|---|---|
| | $TAR_{FA}$ (terrigenous to aquatic ratio) | ratio of long-chain to short-chain fatty acids reflects input of terrestrial organic matter (high values) | Konechnaya et al. (2022) |
| **terpenoids** | sesquiterpenes (isolongifolene/longifolene) | indicator used to trace inundation in coastal pine forests (e.g., *Pinus thunbergii*) | Shinozaki et al. (2022) |
| | triterpenes (squalene, des-A-lupane) | triterpenoids are plant-derived tracing terrestrial vegetation | Alpar et al. (2012) Komeiji et al. (2025) |
| | diterpenes (sclareoloxide) | diterpenes generally suggest vegetation/resin input, this specific compound is an oxidation product of the plant diterpene sclareol | Komeiji et al. (2025) |
| | other terpenoids (1-oxaspiro[2.5]octane 5,5-dimethyl-4-(3-methyl-1, 3-butadienyl)-) | spiro-terpenoids tentatively assigned as plant-derived is an emerging marker with still-developing source specificity | Komeiji et al. (2025) |
| **alkenones** | alkenones ($C_{37}$ unsaturated ketones) | marine indicator produced by certain marine algae (coccolithophores); rarely detected in tsunami deposits due to degradation or low concentrations | Shinozaki et al. (2015) Komeiji et al. (2025) |
| ***n*-aldehydes** | long-chain aldehydes ($C_{24}$-$C_{32}$) | indicator for soil erosion and redeposition originating from plant waxes | Bellanova et al. (2020, 2023) Frenken et al. (2022a) |
| | short-chain aldehydes ($C_{16}$-$C_{22}$) | indicator for marine/aquatic organic matter from algae or microbial activity | Konechnaya et al. (2022) |
| | $EOP_{ALD}$ (even-to-odd predominance) | calculated as $(\sum nC_{24}\text{-}nC_{32})/(\sum nC_{23}\text{-}nC_{31})$, the even-over-odd-dominance of *n*-aldehydes ($EOP_{ALD}$) indicates with high values leaf-wax-derived organic matter and with low values secondary or diagenetic origin | Frenken et al. (2022a) |
| | $TAR_{ALD}$ (terrigenous to aquatic ratio) | calculated as $(\sum nC_{22}\text{-}nC_{24})/(\sum nC_{16}\text{-}nC_{18})$, the $TAR_{ALD}$ indicates with high values terrestrial plant-wax inputs relative to aquatic/algal input | Bellanova et al. (2023) |
| **bulk proxies** | total organic carbon (TOC)/loss of ignition (LOI) | concentration of organic carbon, both TOC and LOI track organic matter content and help to separate different stratigraphies | Shinozaki et al. (2016, 2022) Bellanova et al. (2019, 2023) Frenken et al. (2022a) |
| | C/N ratio | ratio of carbon to nitrogen distinguishing terrestrial from marine organic matter | Chagué-Goff et al. (2012) |
| | $\delta^{13}C$ | stable carbon isotope ratio distinguishing terrestrial $C_3$ plants from marine phytoplankton | Chagué-Goff et al. (2012) Pilarczyk et al. (2012) Shinozaki et al. (2016) |
| | $\delta^{15}N$ | stable nitrogen isotope ratio providing information on nitrogen sources and trophic levels | Chagué-Goff et al. (2012) |
| **novel proxies** | environmental DNA (eDNA) | analysis of genetic material from organisms allows for high-resolution taxonomic identification providing environmental information | Szczuciński et al. (2016) Hiraoka et al. (2016) Yap et al. (2021, 2023) Shinozaki et al. (2025) |

and bacteriohopanepolyols, respectively, are exceptionally stable (e.g., Peters et al., 2005). Their distributions (e.g., $C_{27}$–$C_{29}$ steranes) can preserve the source information of their precursors long after the original sterols have degraded (Bellanova et al., 2023). Specifically, the sterane/hopane (S/H) ratio increases with eukaryotic contributions (lower values indicate bacterial dominance; Gonçalves, 2002; Sepúlveda et al., 2009), while the hopane isomer ratio Ts/Tm is sensitive to depositional environment and organic-matter source (Table 1; Peters and Moldowan, 1993). In combination, these ratios help discriminate marine-influenced tsunami layers from terrestrial background units (Bellanova et al., 2023). Similarly, isoprenoids like pristane and phytane, diagenetic products of chlorophyll, can provide insights into both marine incursions and paleo-redox conditions (pr/ph ratio) (Table 1; Alpar et al., 2012; Bellanova et al., 2023).

Overall, organic lipid biomarkers have emerged as powerful, source-diagnostic tools that complement sedimentological approaches in identifying tsunami deposits and reconstructing inundation, transport pathways, and sediment provenance. Biomarkers have been overwhelmingly validated on modern tsunami deposits, particularly those from the 2011 Tōhoku-oki event (Shinozaki et al., 2015, 2022; Bellanova et al., 2020, 2021; Frenken et al., 2022a; Konechnaya et al., 2022). Despite the rich paleotsunami archive along the Japanese coast, the application of lipid biomarkers to paleotsunami records in Japan (e.g., Komeiji et al., 2025) remains limited. This is also the case in other coastal zones with known paleotsunami records (e.g., Alpar et al., 2012; Ünlü et al., 2012; Mathes-Schmidt et al., 2013).

## 3. Case study area and methodology

### 3.1. Study area

The study area is located in the Maita River Valley (Fig. 1), south of Noda Village (Iwate Prefecture) on the northern Sanriku coast (Japan). In contrast to the well-studied historic and paleotsunami records of the Sendai and Ishinomaki plains (e.g., Minoura and Nakaya, 1991; Minoura et al., 2001; Sugawara et al., 2001, 2012, 2013; Sawai, 2007; Sawai et al., 2008, 2012, 2015; Shishikura, 2007; Satake, 2008; Namegaya et al., 2010), the Sanriku coast exhibits limited written tsunami

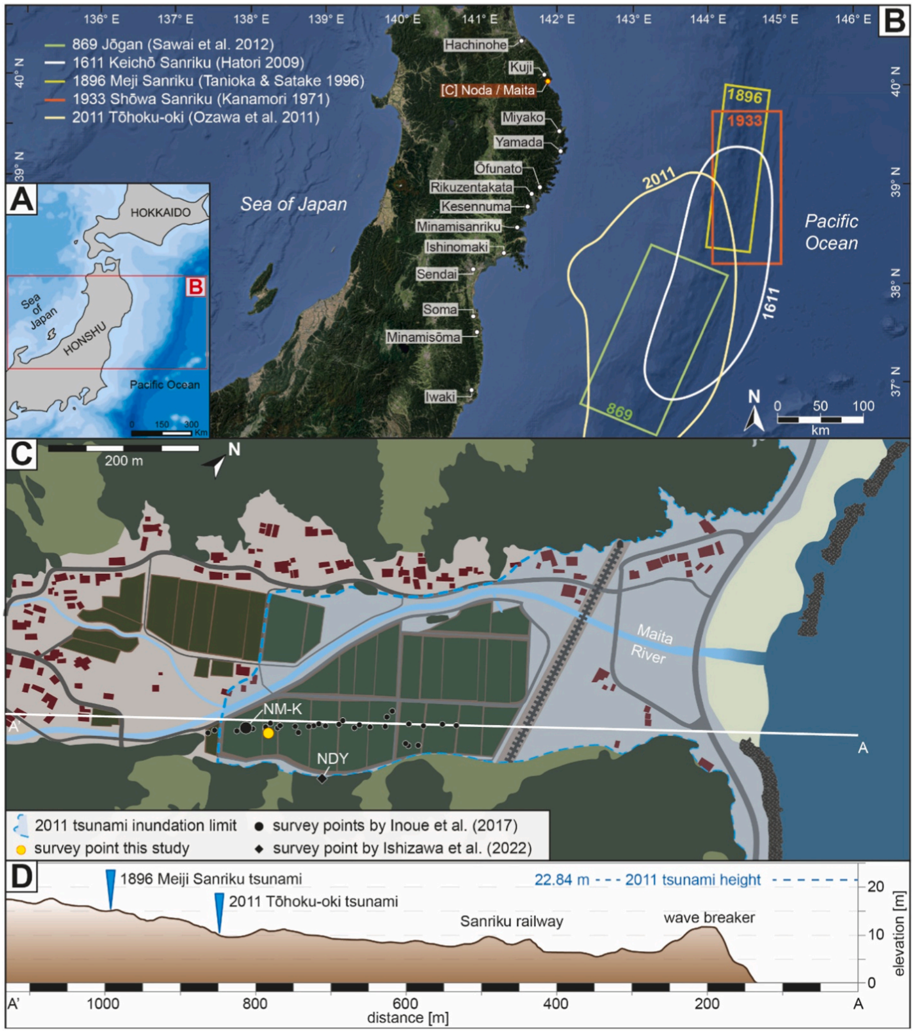


**Fig. 1.** Setting of the Maita River Valley (Noda Village, Sanriku coast, Iwate Prefecture, Japan). (A) Index map of Japan showing the study region on NE Honshu (box in B). (B) Sanriku coastline and offshore source/rupture areas of major historical tsunamis (modified after Inoue et al., 2017): 869 Jōgan (after Sawai et al., 2012), 1611 Keichō Sanriku (after Hatori, 2009), 1896 Meiji Sanriku (after Tanioka and Satake, 1996), 1933 Shōwa Sanriku (after Kanamori, 1971), and 2011 Tōhoku-oki (outlines after Ozawa et al., 2011). (C) Detailed map of the Maita River Valley and coastal plain showing the 2011 Tōhoku-oki tsunami inundation limit (blue dashed line), survey points from Inoue et al. (2017) with the NM-K site marked, the NDY coring size from Ishizawa et al. (2022), and the survey point from this study (yellow). (D) Topographic profile A–A′ across the valley from the shoreline inland (data source: GoogleEarthPro), with the locations of the railway and wave breaker and the observed inundation limits for the 1896 CE and 2011 CE tsunamis.

records prior to the 1933 CE Shōwa Sanriku and 1896 CE Meiji Sanriku tsunamis (Inoue et al., 2017; Goto et al., 2021) and fewer paleotsunami studies. The earliest documented historical tsunami along the Sanriku coast is the 1611 CE Keichō Sanriku tsunami, which is described in written records (Tetsuka et al., 2021) and is also commemorated by a stone tablet in the town center of Miyako city. Historically well-documented in written records is the 1896 CE tsunami along the Sanriku coastline (e.g., Satake et al., 2017). Furthermore, the oldest tsunami monument close to the study area in Noda Village, located at a temple, states that a massive tsunami struck Noda Village in 1896 CE, causing extensive damage with 138 houses lost, 62 injuries, and 261 fatalities (Geospatial Information Authority of Japan, 2025). Despite the limited written record, up to 12–14 historic and paleotsunami deposits during the past 4000 years are known from the Sanriku coast (e.g., Goto et al., 2015, 2019; Ishimura and Miyauchi, 2015; Takada et al., 2016; Inoue et al., 2017; Ishimura, 2017; Ishizawa et al., 2022). Recurrence intervals for tsunamis along the Sanriku coast vary between ~600 years (Sawai et al., 2015), ~400 years (Ishizawa et al., 2022), and 350–390 years (Ishimura, 2017). However, as Inoue et al. (2017) point out, the Sanriku coast is disadvantaged for paleotsunami research, with low sedimentary potential and a lack of extensive coastal lowlands due to its mountainous and river-valley topography. This coastal setting with steeply incised ria coastlines can amplify tsunami wave heights and channel floodwaters far inland during extreme events (Inoue et al., 2017).

The Maita area is a narrow valley opening eastwards to the Pacific Ocean (Fig. 1). The bed of the Maita River is up to ~5 m wide (Inoue et al., 2017) traversing through urban and agricultural areas of rice paddies. The present-day beach is composed mainly of gravel and sand (Inoue et al., 2017). Prior to the 2011 Tōhoku-oki tsunami, two wave breakers were located at ~50 m and ~300 m from the coast, with the latter being the elevated tracks of the Sanriku railway (Fig. 1; Inoue et al., 2017). The 2011 tsunami impacted the Maita area, reaching up to ~720 m inland (Fig. 1; Inoue et al., 2017). Notably, numerical storm wave modeling by Inoue et al. (2017) demonstrated that even the extreme storm conditions at this site produced a maximum onshore inundation of only ~450 m. After the 2011 tsunami, both wave breakers were reinforced with concrete, and a third wave breaker was built inland of the Sanriku railway tracks.

Inoue et al. (2017) and Ishizawa et al. (2022) studied the sedimentary tsunami record of the Maita River Valley (Fig. 1). Both studies identified four (Inoue et al., 2017) and five tsunami deposits (Ishizawa et al., 2022), respectively, with the oldest deposits dating back up to ~2700 years.

The well-defined temporal constraints and sedimentological characterization of these paleotsunami deposits (Inoue et al., 2017; Ishizawa et al., 2022) render the Maita River Valley a suitable study site to apply, test, and review lipid biomarkers on some of the few well-studied paleotsunami deposits of the Sanriku coastline (e.g., Goto et al., 2015, 2019; Ishimura and Miyauchi, 2015; Takada et al., 2016; Inoue et al., 2017; Ishimura, 2017; Ishizawa et al., 2022).

### 3.2. Field survey, sample collection and description

The field survey took place in February 2018, when the alluvial lowland was not used for rice cultivation, but after the 2011 tsunami debris and deposits had been removed.

A 68 cm-long handy geoslicer (Nakata and Shimazaki, 1997; Takada et al., 2002) was taken ~650 m from the present-day coast, clearly beyond the local storm inundation limit at ~450 m (Inoue et al., 2017) and 350 m from the landward-most tsunami wave breaker (Fig. 1). The site is within 25 m seaward of the NM-K core location of Inoue et al. (2017) and within 100 m of the NDY core location of Ishizawa et al. (2022), where historic and prehistoric tsunami deposits were recovered, described and dated. The sediment core was cleaned, photographed, and described before samples were taken using pre-cleaned metal tools.

### 3.3. Bulk analyses (grain size and TOC)

For grain size analysis via laser diffraction (Laser Diffraction Particle Size Analyzer – Beckman Coulter LS 13 320), a total of 18 samples were prepared by drying (40 °C for 48 h), sieving (<2 mm), pretreated with hydrogen peroxide ($H_2O_2$, 15%) to remove organic matter, and with sodium pyrophosphate ($Na_4P_2O_7$) to avoid flocculation (Gee and Or, 2002). Laser diffraction grain-size measurements were performed three times in 116 channels from 0.4 to 2000 μm. The results were statistically processed using GRADISTAT software version 9.1 (Blott and Pye, 2001) using the logarithmic (phi-scale) method of Folk and Ward (1957).

For total organic carbon (TOC) determination, ca. 1 g of sample material was dried, homogenized, and 100 mg was weighed into a quartz boat for analysis. TOC was measured using the liquiTOC II (Elementar Analysesysteme GmbH, Germany) in single-analytical-run mode. Calibration was performed before every measurement.

### 3.4. Extraction and quantification of organic compounds

To analyze and quantify a broad suite of environmentally sensitive lipid biomarkers, collected samples were subjected to solid-liquid extraction followed by fractionation to maximize detectability in subsequent high-resolution GC-MS analyses.

A representative aliquot of 34 to 82 g wet sediment (n = 18) was extracted three times using overhead shaking and ultrasonic agitation: (1) with 110 mL acetone for 4 h, (2) with 110 mL acetone for 24 h, (3) with 110 mL *n*-hexane for 24 h. The resulting extracts were separated from the sediment via centrifugation and combined in a separatory funnel. The sample extracts were reduced via rotary evaporation (300 mbar), and the aqueous phase was removed through a surplus of *n*-hexane and drying over anhydrous granulated sodium sulfate. Further, the extracts were desulphurized with activated copper powder and ultrasonic agitation.

Before gas chromatography-mass spectrometry, sample extracts were fractionated into six portions (B1–B6) by column chromatography (Franke et al., 1998). Sequential elution used mixtures of *n*-pentane, dichloromethane (DCM) and methanol (MeOH): (I) *n*-pentane for aliphatic hydrocarbons; (II) *n*-pentane/DCM 95:5 for monoaromatics; (III) *n*-pentane/DCM 90:10 for diaromatics; (IV) *n*-pentane/DCM 40:60 for polyaromatics; (V) DCM for semipolar compounds; and (VI) MeOH for polar compounds (Schwarzbauer et al., 2000). The acidic constituents in B6 were methylated with $BF_3$-MeOH following Bellanova et al. (2024). Alcohols were then derivatized by acetylation using acetic anhydride and pyridine. Each sample fraction was spiked with 50 μL of internal surrogate standard (5.8 ng/μL fluoracetophenone, 6.28 ng/μL $d_{10}$-benzophenone, and 6.03 ng/μL $d_{34}$-hexadecane).

For compound identification and quantification, all sample fractions were measured by gas chromatography-mass spectrometry (GC-MS). Measurements were performed on a quadrupole, GC-MS instrument (Thermo Finnigan Trace GC-MS) with helium as carrier gas and equipped with a 30 m × 0.25 mm i. d. × 0.25 μm film ZB-5 fused silica capillary column (Zebron capillary GC column Chrompack). 1 μL of each sample was injected at an initial temperature of 60 °C with a splitless time of 60 s, a temperature hold of 3 min, followed by a temperature ramp of 3 °C/min to 310 °C and another hold for 20 min. The mass spectrometer operated in full-scan mode, achieving a range from 35 to 500 m/z (mass-to-charge ratio) in positive electron impact ionization mode ($EI^+$) with 7 eV.

Identification of individual compounds was achieved, comparing EI + mass spectra with mass spectral databases (NIST, Wiley). Compound identification was verified with mass spectral parameters of purchased standard reference materials. Organic compound concentrations were quantified by integrating characteristic ion chromatograms extracted from the total ion current. Response factors were determined using four-point linear regression functions derived from external calibration measurements. Inaccuracies arising from injection and sample-volume variability were corrected using the internal surrogate standard. Limits of detection (LoD) were set at signal-to-noise ratios >3, and limits of quantification (LOQ) at >10. Since target analytes were not detected in blanks (see QA/QC section), blank corrections were not applied.

### 3.5. Quality assurance and quality control (QA/QC)

In all sampling and analytical processing steps, solely pre-cleaned glass or metal tools were used to minimize contamination. Gas chromatographic analyses tested solvent purity. Anhydrous granulated $Na_2SO_4$ and hydrochloric acid were cleaned with pure solvents before usage. Sample storage temperature below −20 °C until geochemical extraction was ensured to avoid microbial alteration of the geochemical signature.

Data quality assurance (QA) and quality control (QC) protocols included laboratory blanks, duplicate samples, and measurements to check for the absence of external contamination. Reference materials for the identified compounds were obtained from Sigma-Aldrich to ensure accuracy and traceability in quantification, and to account for compound-specific gas chromatographic retention times and elution orders. While established quality control measures limit analytical inaccuracies, natural variations (e.g., TOC content and grain size) need to be considered (Frenken et al., 2022a). To reduce adverse effects, samples have been homogenized before extraction, and concentrations normalized to TOC content.

## 4. Results and interpretation

### 4.1. Sedimentological characterization

The 68 cm-long sediment core retrieved from the Maita River Valley exhibits seven stratigraphic units (L1–L7), which are interbedded with four distinct sand beds (E-I to E-IV; Fig. 2).

#### 4.1.1. Unit L1 (0–5 cm depth)

The uppermost unit consists of a dark brown (Munsell color 2.5 YR 5/2) silt with abundant plant matter (Fig. 2), reflected in the relatively

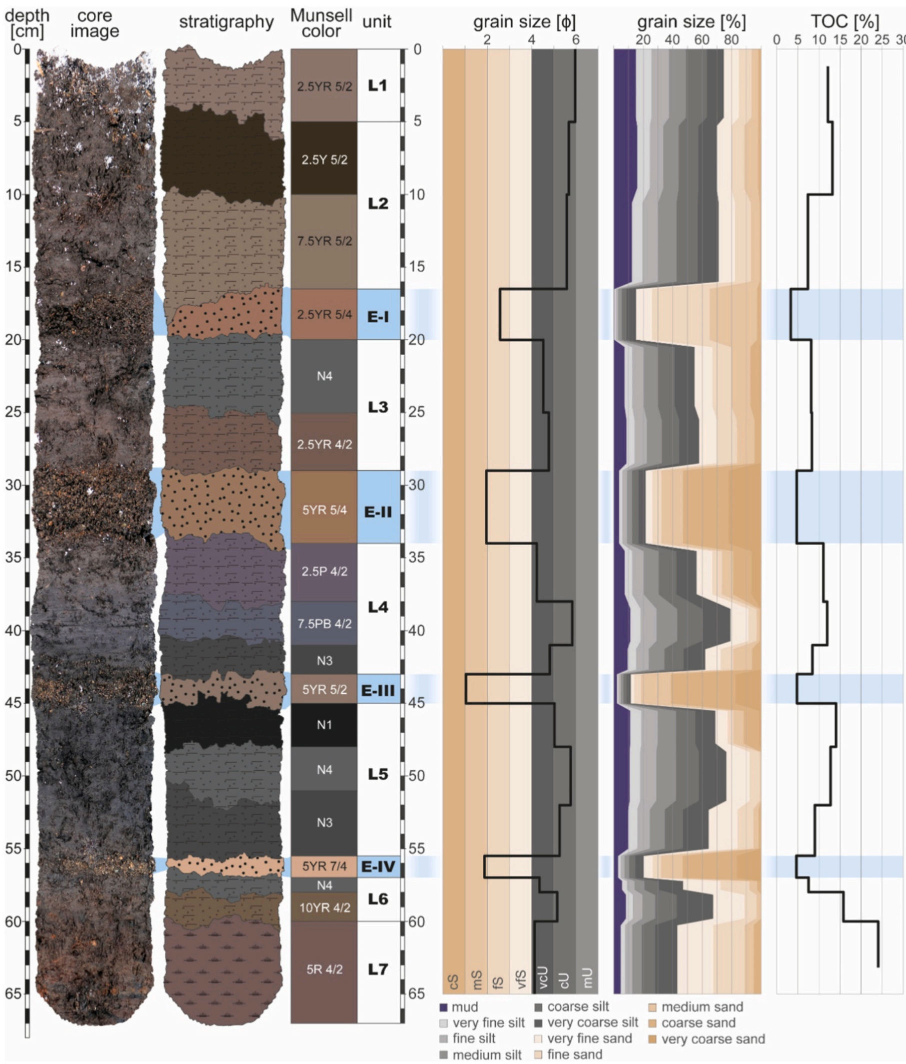


**Fig. 2.** Down-core sedimentological characterization of the sediment core. Left: Core image, stratigraphy/lithology interpretation, Munsell color and stratigraphic unit description with the four event layers (E-I to E-IV) being highlighted in blue. Right: Grain size distribution showing mean grain size [Φ], grain size distribution [%], and total organic carbon (TOC) [%].

high organic carbon content (TOC 12%; Table S1). The mean grain size (5.97 Φ) corresponds to coarse silt, and the sediment is very poorly sorted (2.7 Φ). The grain-size distribution is dominated by silt (60%), with sand (26%) and mud (15%) being minor components. The unit is bioturbated by roots, and no lamination was observed. This unit represents the contemporary agriculturally disturbed soil of the rice paddy field from which the core was retrieved.

#### *4.1.2. Unit L2 (5–16.5 cm depth)*

The second unit comprises two sub-layers separated by subtle color changes. The upper sub-layer (L2.1; 5–10 cm) is a dark gray (2.5Y 5/2) silt with abundant roots. The lower sub-layer (L2.2; 10–16.5 cm) is a brownish (7.5 YR 5/2) silt. TOC values decrease from 13.2% in L2.1 to 7.3% in L2.2, reflecting the lack of roots in the lower section of the unit. Mean grain size is a coarse silt (5.59–5.69 Φ) with very poor sorting (2.77–2.93 Φ). Silt-sized particles account for ~54–59% of the sediment composition, with sand (29–30%) and mud (12–16%) being minor components. During fieldwork, a patchy vein of volcanic ash was described in the lower parts of the unit (~15 cm; Fig. 2), but it was too thin to be sampled separately. This volcanic ash bed corresponds to previous stratigraphic descriptions of Inoue et al. (2017), who detected and dated a volcanic ash deposit in the upper 20 cm of the Maita stratigraphy.

#### *4.1.3. Unit E-I (16.5–20 cm depth)*

This unit is composed of a 3–4 cm-thick reddish brown (2.5 YR 5/4) sand that fines upward. The contact with the underlying unit is erosional, and silt clasts occur at the base of unit E-I. The upper contact to unit L2 is sharp and marked by a change in color and grain size. Both contacts indicate an abrupt shift in the depositional environment. The mean grain size of unit E-I is 2.58 Φ (fine sand) with poor sorting (1.34 Φ). Sand constitutes 85% of the material, dominated by fine (39%) and medium (32%) sand, as well as very fine sand (11%) and coarse sand (3%) as minor components. Silt (15%) is a minor component. Visually, the sand is dominated by light-colored grains (e.g., quartz and feldspar), accompanied by sparse dark heavy mineral grains (e.g., mica, pyroxene, magnetite). No marine bioclasts (shell fragments or foraminifera) were identified within this layer. Furthermore, the organic carbon content is markedly lower (TOC 3.3%) than in adjacent units.

#### *4.1.4. Unit L3 (20–29 cm depth)*

The third unit comprises two sub-units, specifically the upper L2.1, a dark gray (N4) silt, and the lower L2.2, a brown (2.5 YR 4/2) silt. Mean grain size ranges from 4.53 to 4.78 Φ (very coarse silt) with very poor sorting (2.80–2.81 Φ). Silt-sized particles account for ~47–49% of the sediment composition with equal contributions of sand (45–42%) and a minor proportion of mud (7–9%). Furthermore, the unit shows lamination of organic-rich matter (TOC 8.1-8.3%) and slight mottling.

#### 4.1.5. Unit E-II (29–34 cm depth)

The ~5 cm thick unit E-II is characterized by a reddish brown (5 YR 5/4) sand intercalated between unit L3 and L4. It exhibits an erosive base and contains reworked silt clasts (rip-up). Likewise, the upper boundary to unit L3 is sharply defined. Mean grain size (1.96 Φ) corresponds to medium sand with a very poor sorting (2.68 Φ). The sand is comprised mainly of coarse (22%) and very coarse sand (31%), as well as medium sand (15%), fine sand (6%) and very fine sand (5%). Silt-sized particles (18%) and mud (3%) are minor components. The mineral composition is consistent with that of E-I, dominated by light minerals (quartz, feldspar) with minor dark heavy mineral grains and reddish-brown weathered lithic particles. Marine bioclasts are absent in unit E-II. TOC values are low (4.7%), reflecting the shift to coarser sediment.

#### 4.1.6. Unit L4 (34–43 cm depth)

The 9 cm thick unit L4 is a heterogeneous silt succession characterized by an internal shift in color and grain size. The uppermost 4 cm-thick section L4.1, sharing an erosive contact with unit E-II, is a dark purple (2.5P 4/2), very poorly sorted (3.19 Φ), very coarse silt (4.24 Φ). The 3 cm-thick middle section L4.2 is a bluish-gray (7.5 PB 4/2), very poorly sorted (2.39 Φ) coarse silt (5.84 Φ). The bottom section L4.3 is a dark gray (N3), very poorly sorted (2.94 Φ), very coarse silt (4.82 Φ). The main components of L4.1 and 4.3 are silt-sized particles (49–53%), followed by sand (38–44%), with minor contributions from mud (7–9%). Sub-unit L4.2 contrasts slightly with a dominance of silt (68%) and smaller contributions of sand (21%) and mud (11%). The TOC ranges from 8.4 to 12.0% indicating organic-rich sediments. The lower sub-units L4.2 and L4.3 show mottling.

#### 4.1.7. Unit E-III (43–45 cm depth)

This ~2 cm-thick horizon is a brown to reddish (5 YR 5/2) sand with an upward-fining trend. Its erosive basal contact truncates into the underlying unit L5 and is marked by small silty rip-up clasts. The deposit has a mean grain size of 1.04 Φ (coarse sand) and poor sorting (1.73 Φ). Sand accounts for 89% of the composition, with coarse and very coarse sand fractions making up >60% of the sand, while silt (9%) and mud (2%) are minor components. The sand fraction of E-III is mineralogically composed of light-colored components (e.g., quartz, feldspar), minor heavy minerals and weathered or oxidized minerals. Furthermore, no marine bioclasts were identified. TOC is 4.77%, much lower than in the surrounding units.

#### 4.1.8. Unit L5 (45–55.5 cm depth)

The ~10.5 cm-thick unit L5 consists of three very dark gray to black (N1–N4) peaty silts. Mean grain size ranges between 5.04 and 5.76 Φ (coarse silt) with generally very poor sorting (2.34–3.24 Φ). Silt (55–65%) is the dominant particle size, followed by sand (24–36%), with minor contributions from mud (10–11%). TOC is high (9–14.1%), but shows a downward decreasing trend from L5.1 to L5.3.

#### 4.1.9. Unit E-IV (55.5–57 cm depth)

The ~1.5 cm-thick unit E-IV is a light brown (5 YR 7/4) medium sand with a mean grain size of 1.88 Φ and very poor sorting (2.44 Φ). Sand (80%) is the dominant particle fraction, followed by silt (17%) and a minor contribution of mud (3%). The mineralogical composition of E-IV is dominated by light-colored grains (quartz, feldspar), with a minor component of dark- and brown-colored grains (heavy minerals and weathered minerals). No marine bioclasts were detected. The layer has a sharp, erosive upper contact. TOC (4.61%) is significantly lower than in the overlying and underlying units L5 and L6.

#### 4.1.10. Unit L6 (57–60 cm depth)

Unit L6 is composed of a dark gray to brown (N4 to 10 YR 4/2) peaty silt. The mean grain size indicates it is a very coarse to coarse silt (4.35–5.16 Φ) with very poor sorting (2.21 Φ). Sand (33–53%) and silt (41–59%) are the dominant components of this unit, with minor contributions from mud (6–8%). TOC is increasing with depth from 7.5 to 15.8%.

#### 4.1.11. Unit L7 (60–65 cm depth)

The lowermost unit L7 is a reddish-brown (5R 4/2) peat. It is a very poorly sorted (2.23 Φ), very coarse silt (4.14 Φ), composed of very coarse sand (1%), coarse sand (5%), medium sand (6%), fine sand (21%), very fine sand (24%), very coarse silt (15%), coarse silt (9%), medium silt (6%), fine silt (5%), very fine silt (3%), and a minor contribution of mud (5%). TOC values are highest (24%), reflecting the accumulation of organic matter in this layer. The transition between units L6 and L7 is transitional.

#### 4.1.12. Sedimentological interpretation

The observed stratigraphies (L1–L7) represent the low-energy fluvial overbank (floodplain) deposits marking the background signature, which is consistent with previously organic-rich sediments described from Maita and Noda (Inoue et al., 2017; Ishizawa et al., 2022). The four intercalated sand beds (E-I to E-IV) contrast with the surrounding organic-rich silts and peats in color, texture, and grain size (Fig. 2; Fig. 3; Table S1). Each event layer exhibits an erosive basal contact, and some show fining-upward grain size trends (E-I and E-III), a pattern commonly observed during high-energy inundation events (e.g., Dawson and Shi, 2000; Morton et al., 2007; Peters and Jaffe, 2010; Goff et al., 2012). Moreover, the presence of coarse sand fractions and silty rip-up clasts indicates a capacity to erode and entrain material from underlying sediments (e.g., Morton et al., 2007; Peters and Jaffe, 2010). The four event beds comprise mixed siliciclastic sand with light mineral grains, dark lithic/heavy-mineral grains and reddish-brown weathered lithic particles. It should be noted that no dedicated mineralogical analysis was conducted in this study, and mineralogical descriptions are limited to visual observations. Notably, this sediment composition resembles modern beach deposits from the Noda coastline, which consist mostly of light-colored sand with a minor heavy mineral component (Fig. S1; Inoue et al., 2017), suggesting a beach sediment source for the event layers.

Importantly, no marine bioclasts (e.g., shell fragments, foraminifera, or diatoms) were identified in any of the four event layers (E-I to E-IV). This contrasts with the description of the contemporary 2011 Tōhoku-oki tsunami deposit at Maita (Noda), in which shell fragments were reported by Inoue et al. (2017). However, low abundance or non-preservation of marine macro- and micro-bioclasts is a common observation in high-energy inundation events including the 2011 Tōhoku-oki tsunami deposits at the Sendai Plain (e.g., Chagué-Goff et al., 2012; Pilarczyk et al., 2012; Szczuciński et al., 2012; Abe et al., 2020) and paleotsunami deposits (e.g., Goff et al., 2012; Garrett et al., 2018; Putra et al., 2023). The absence of calcareous bioclasts in the event layers does not preclude a marine inundation origin. However, it may reflect carbonate dissolution in the organic-rich, mildly acidic peat depositional environment over millennial timescales (e.g., Chagué-Goff et al., 2012; Hawkes, 2020; Szczuciński, 2020; Putra et al., 2023).

Overall, these properties (e.g., erosive basal contacts, fining-upward grain-size trends, rip-up clasts) are consistent with those commonly reported for tsunami deposits (e.g., Dawson and Shi, 2000; Morton et al., 2007; Peters and Jaffe, 2010; Goff et al., 2012), and the number of detected layers, their stratigraphic position, and grain size signature correspond to those described in the nearby NM-K core by Inoue et al. (2017) and the NDY core taken in a forested area adjacent to the rice paddies by Ishizawa et al. (2022), supporting a tsunami interpretation (Fig. 3). This stratigraphic correlation of the four event layers (E-I to E-IV) with recognized paleotsunami deposits from the same valley provides provisional chronological control (Fig. 3), based on the radiocarbon and tephra dating conducted by Inoue et al. (2017) and

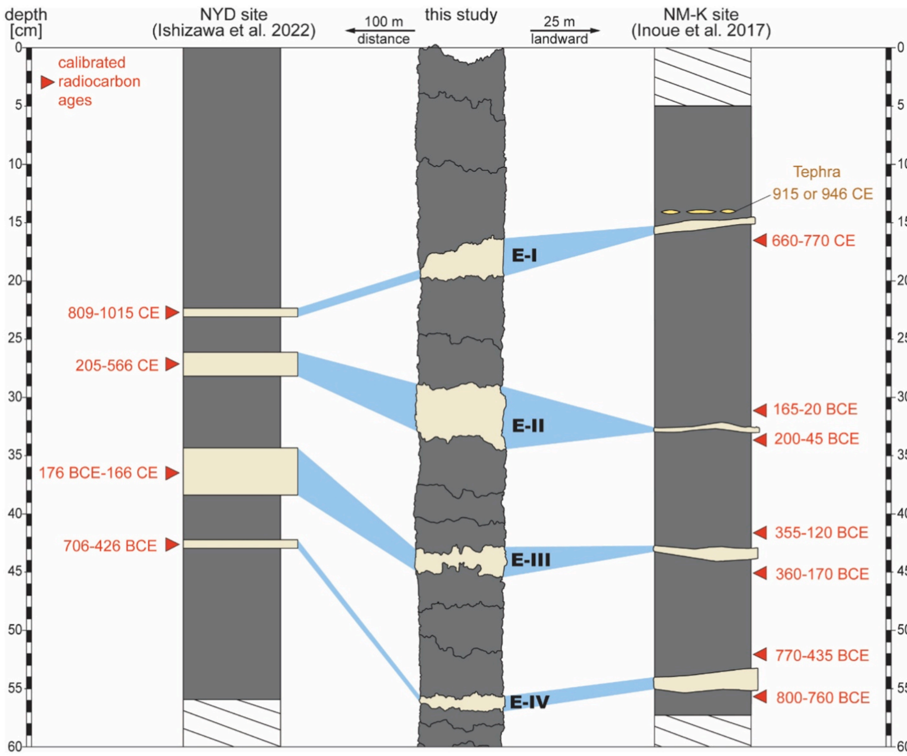


**Fig. 3.** Tentative chronostratigraphic correlation of the 68 cm-long sediment core from the Maita River Valley analyzed in this study with nearby published stratigraphies and radiocarbon ages from the NM-K site (ca. 25 m distance) after Inoue et al. (2017) and from the NDY site (ca. 100 m distance) after Ishizawa et al. (2022). Blue bands indicate the correlation between the four event layers identified in this study and the previously described paleotsunami deposits.

Ishizawa et al. (2022). However, because these published sequences were obtained from less-disturbed settings (forested sites in Ishizawa et al., 2022) or predate major land modification (Inoue et al., 2017), and because the present core does not contain clear volcanic tephra beds, the age correlation should be considered tentative. Based on this correlation the four event layers are approximately placed as follows (Fig. 3): E-I (~915/946–770 CE or 809–1015 CE), E-II (200–20 BCE or 205–566 CE), E-III (360–120 BCE or 176 BCE–166 CE), and E-IV (800–435 BCE or 706–426 BCE). The event layer E-I (16.5–20 cm depth) may potentially correspond to a known historic event, the 869 CE Jōgan tsunami, based on the stratigraphic position below a very thin patchy vein of volcanic ash (L2). This volcanic ash may be correlated to either the 915 CE Towada eruption and resulting To-a tephra (e.g., Sawai et al., 2008) or the 946 CE eruption of Changbaishan volcano resulting in the B-Tm tephra (e.g., Oppenheimer et al., 2017), both being reported from the nearby NM-K sequence (Inoue et al., 2017). Event layers E-II, E-III, and E-IV record large undocumented prehistoric paleotsunamis. It must be noted that all four event layers (E-I to E-IV) are inferred to represent paleotsunami deposits on the basis of their stratigraphic correspondence with the NM-K and NDY sequences; however, without direct dating of the present core, individual age assignments and specific event correlations cannot be confirmed.

Overall, this study's sedimentological observations (grain size, texture, erosive contacts, etc.) and interpretation of the four sand layers as being of tsunami origin are consistent with previously reported local stratigraphies from the Maita River Valley (Inoue et al., 2017; Ishizawa et al., 2022) and with the regional context of paleotsunami deposit distributions along the Sanriku coast (e.g., Goto et al., 2015, 2019; Ishimura and Miyauchi, 2015, 2017; Takada et al., 2016; Inoue et al., 2017; Ishimura, 2017; Ishizawa et al., 2022). Furthermore, as mentioned in Section 3.2, the core was taken beyond the limit of the maximum modelled storm inundation, thus suggesting that a storm origin can be excluded.

### 4.2. Sedimentary biomarkers

A diverse suite of lipid biomarkers was identified (Fig. 4) and quantified across all sediment samples of the geoslicer from the Maita River Valley. The detected compound classes include homologous series of *n*-alkanes, *n*-aldehydes, and fatty acids, as well as terpenoids, steranes, and hopanes (Table S2).

#### 4.2.1. *n*-Alkanes and isoprenoids

The homologous series of *n*-alkanes ranging from $C_{11}$ to $C_{35}$ were detected throughout the sediment core, with both short-chain ($C_{11}$–$C_{21}$) and long-chain ($C_{25}$–$C_{35}$) homologues present in all samples (Fig. 4; Fig. 5; Table S2). Total *n*-alkane concentrations ($\sum$*n*-alkanes in $\mu g/g_{TOC}$) are distinctively elevated within all four event layers (E-I to E-IV) compared to the background sediments (peat and silt) (Fig. 5). This increase is driven primarily by a significant rise in short-chain *n*-alkanes ($\sum C_{11}$–$C_{21}$ *n*-alkanes in $\mu g/g_{TOC}$). While these compounds are ubiquitous and originate from algae and bacteria, they are also commonly associated with marine or aquatic sources (e.g., Volkman et al., 1998). Consequently, the terrigenous-to-aquatic ratio ($TAR_{ALK}$) drops sharply within all four event layers to values < 6.4 (Fig. 5; Table S2). This distinguishes them from the strongly terrestrial-dominated background peat and silt layers with average $TAR_{ALK}$ values ranging from 8.5 to 17.6. These suppressed TAR values in the event layers reflect enhanced relative contributions of short-chain *n*-alkanes derived from marine and aquatic sources, consistent with marine inundation during tsunami events (Shinozaki et al., 2015; Bellanova et al., 2021).

The odd-even predominance ($OEP_{ALK}$) and carbon preference index ($CPI_{ALK}$) values for *n*-alkanes range from 1.1 to 2.3 and 1.4–3.2, respectively, across the sediment profile (Table S2). Both show parallel trends (Fig. 5) with notably elevated values in the event layers ($OEP_{ALK}$: 2.0–2.3; $CPI_{ALK}$: 2.4–3.2) compared to the adjacent background sediments ($OEP_{ALK}$: 1.1–1.6; $CPI_{ALK}$: 1.4–2.4). This suggests that the organic matter incorporated in the event deposits is undegraded compared to the

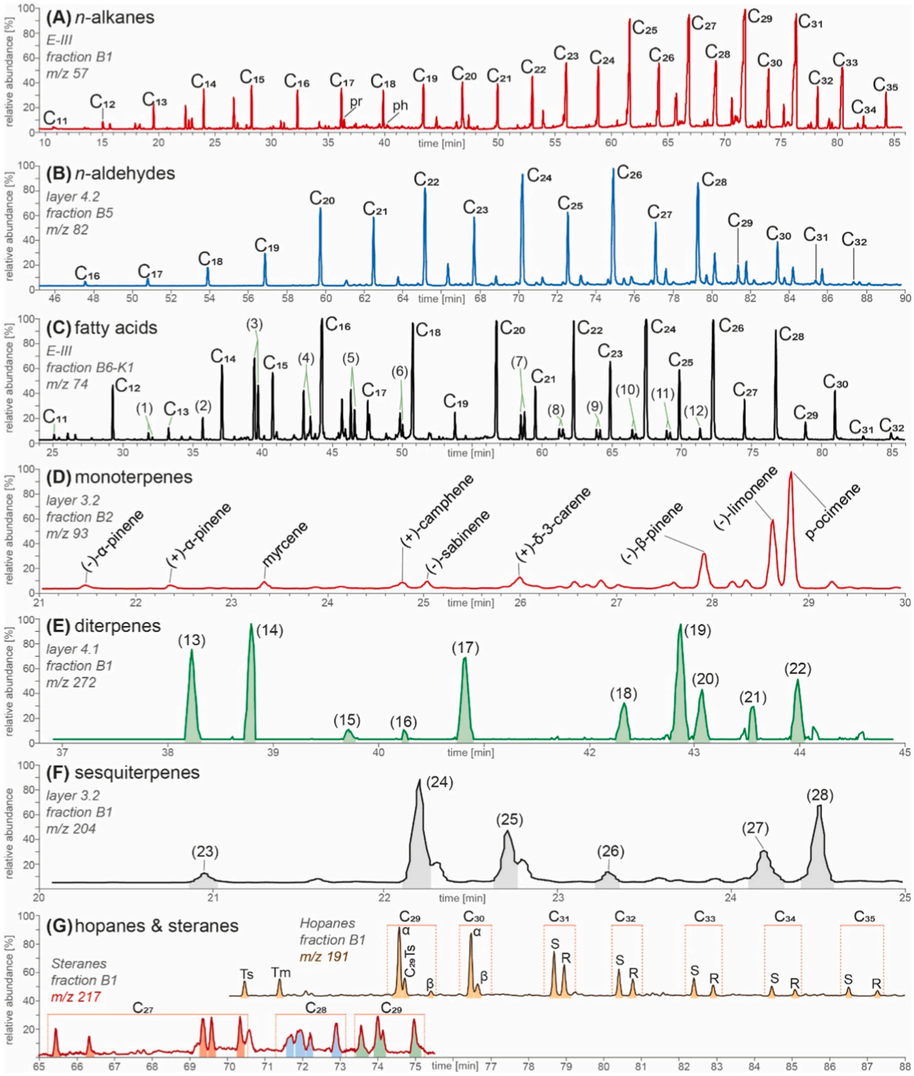


**Fig. 4.** Representative GC-MS chromatograms of (A) *n*-alkanes and isoprenoids (pr, ph) (m/z 57), (B) *n*-aldehydes (m/z 82), (C) fatty acids or their respective fatty acid methyl esters (FAMEs) (m/z 74), terpenoids divided into (D) mono- (m/z 93), (E) di- (m/z 272) and (F) sesquiterpenes (m/z 204), and (G) hopanes (m/z 191) and steranes (m/z 217). Additional numbers indicate (1) iso- & anteiso-$C_{13}$ FA, (2) anteiso-$C_{14}$ FA, (3) iso- & anteiso-$C_{15}$ FA, (4) anteiso-$C_{16}$ FA & palmitoleic acid, (5) iso- & anteiso-$C_{17}$ FA, (6) phytanic acid & oleic acid, (7) iso- & anteiso-$C_{21}$ FA, (8) iso- & anteiso-$C_{22}$ FA, (9) iso- & anteiso-$C_{23}$ FA, (10) iso- & anteiso-$C_{24}$ FA, (11) iso- & anteiso-$C_{25}$ FA, (12) iso- & anteiso-$C_{26}$ FA. Numbers (13–22) mark unresolved but quantified peaks in the diterpene chromatogram and (23–28) mark unresolved but quantified peaks in the sesquiterpene chromatogram.

more microbially degraded organic matter in the background sediments, reflecting inputs of relatively fresh higher-plant material entrained during tsunami inundation (e.g., Bellanova et al., 2020).

The isoprenoids pristane and phytane, derived from phytol (e.g., Rontani and Volkman, 2003), were detected in all samples. The diagnostic redox indicator of the pristane/phytane (pr/ph) ratio varies considerably throughout the core, ranging from 0.2 to 3.3 (Table S2). The pr/ph ratio is notably low (≤0.7) in all four event layers, contrasting with the higher, more variable values (1.5–3.3) of the background peat and silt. Low pr/ph ratios (<1) are indicative of more reducing (anoxic/sub-oxic) depositional conditions, while higher values (>3) indicate oxic conditions (e.g., Didyk et al., 1978). The reduced pr/ph values of the event layers (Fig. 5) are consistent with more reducing depositional conditions or enhanced marine phytoplanktonic input during tsunami inundation (e.g., Alpar et al., 2012; Bellanova et al., 2023). Such low pr/ph ratios in event layers can be attributed to the entrainment and transport of sub-oxic to anoxic seafloor sediments by the tsunami wave. Such marine sediments typically become anoxic within the uppermost few centimeters regardless of bottom-water oxygen conditions (e.g., Didyk et al., 1978), in which the reductive, phytane-forming diagenetic pathway from chlorophyll-derived phytol dominates over the oxidative, pristane-forming pathway (Rontani and Volkman, 2003; Rontani and Bonin, 2011). Furthermore, the rapid burial of transported marine organic debris (e.g., phytoplankton) promotes locally reducing conditions post-deposition, as oxygen is rapidly consumed during microbial degradation of this organic matter, further favoring phytane over pristane formation (e.g., Watanabe et al., 2020).

The cross-plot of pristane/*n*-$C_{17}$ versus phytane/*n*-$C_{18}$ (Fig. 6) is a common proxy for delineating the sources of organic matter and for providing information on the depositional redox environment and diagenetic modifications, such as biodegradation and thermal maturity (Shanmugam, 1985; Hunt, 1996; Peters et al., 2005). The diagnostic cross-plot clearly segregates the samples by facies. Notably, the event layer (E-I to E-IV) data points are tightly clustered within the field of aquatic organic matter. In contrast, the background units occupying a broader range within the threshold are indicative of terrigenous organic matter. Such variations in pr/*n*-$C_{17}$ vs. ph/*n*-$C_{18}$ can result from external input of oxidized organic matter (Didyk et al., 1978; Goossens et al.,

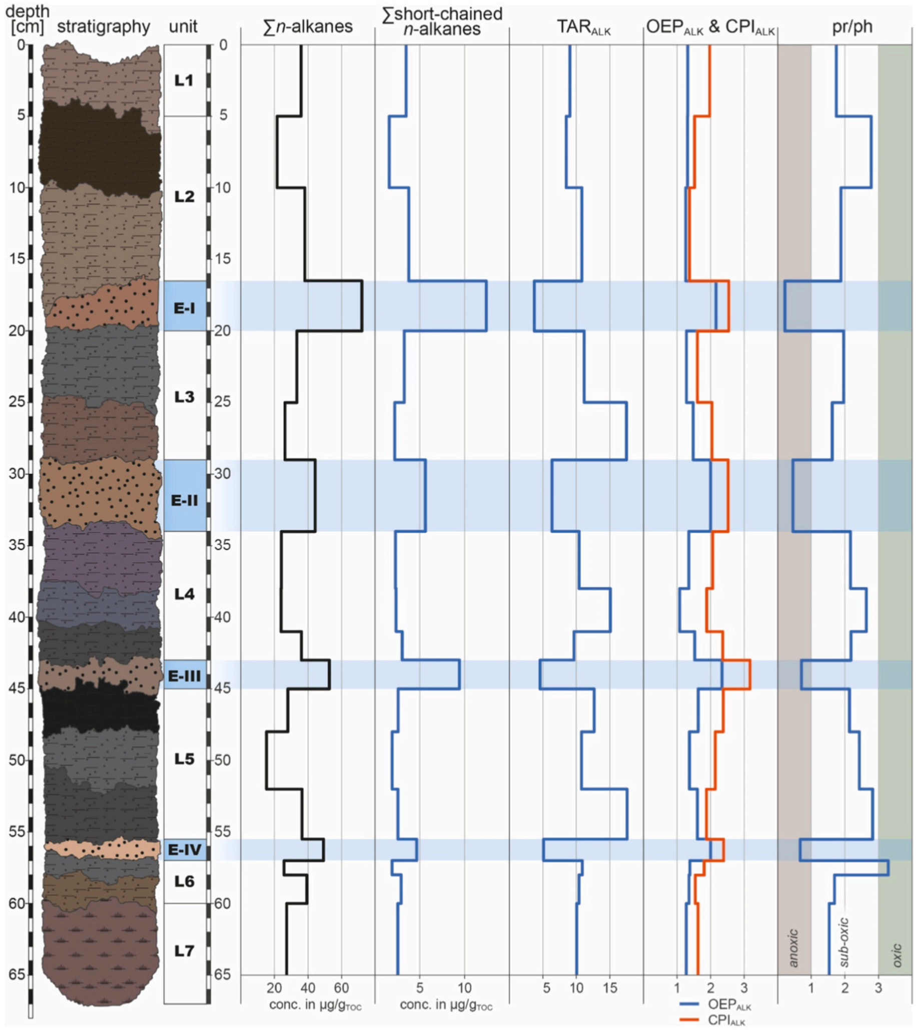


**Fig. 5.** Downcore distribution of *n*-alkanes and isoprenoids, and their diagnostic ratios. From left to right: core stratigraphy, stratigraphic units and downcore profiles of *n*-alkanes and isoprenoids. Presented are the Σ*n*-alkanes (in $\mu g/g_{TOC}$), Σshort-chained ($nC_{11}$-$nC_{21}$) *n*-alkanes (in $\mu g/g_{TOC}$), terrigenous-to-aquatic ratio ($TAR_{ALK}$), odd-even predominance ($OEP_{ALK}$; in blue) and carbon preference index ($CPI_{ALK}$; in orange), and the isoprenoid ratio of pristane/phytane (pr/ph). Blue shades indicate the event layers (E-I to E-IV) interpreted as tsunami deposits.

1984; Powell, 1988). However, cross-referencing with the $OEP_{ALK}$ and $CPI_{ALK}$ indicates a fresh/immature input of organic matter (e.g., Scalan and Smith, 1970; Marzi et al., 1993; Bush and McInerney, 2013; Thomas et al., 2021); therefore, alterations from oxidized organic matter can be excluded. The distribution pattern of event deposits is characteristic of organic matter from marine or aquatic sources, with minimal biodegradation under reducing conditions, consistent with rapid deposition and burial during tsunami inundation events. Cross-plot results resonate with observations from the isoprenoid pr/ph ratio and *n*-alkanes (e.g., short-chain *n*-alkanes or $TAR_{ALK}$).

#### 4.2.2. *n-Aldehydes*

The homologous series of *n*-aldehydes ($C_{16}$–$C_{32}$) was identified in all samples of the sediment profile (Fig. 4). Total *n*-aldehyde concentrations (∑*n*-aldehydes) range from 15.4 to 72.2 $\mu g/g_{TOC}$ (Table S2). *n*-Aldehydes are generally considered plant-derived biomarkers, particularly long-chain congeners ($C_{26}$–$C_{32}$), which are introduced into sedimentary systems by land-plant waxes (Prahl and Pinto, 1987). The medium-chained congeners ($C_{23}$–$C_{25}$) are important components of plant-based essential oils (Fahlbusch et al., 2003), whereas the environmental allocation of the short-chain *n*-aldehydes ($C_{16}$–$C_{23}$) is not fully resolved (Prahl and Pinto, 1987). However, short-chained *n*-aldehydes are tentatively associated with aquatic or microbial sources (c.f., Konechnaya et al., 2022). Across the samples from the Maita River Valley, the short-chain *n*-aldehydes show pronounced concentration peaks ranging from 632 to 1503 $ng/g_{TOC}$ in event layers (Fig. 7; Table S2). These elevated concentrations in the sandy event layers likely reflect the input of marine and aquatic organic matter during tsunami inundation. This observation is reflected in the balance of long-chain to short-chain *n*-aldehydes and the terrigenous-to-aquatic ratio ($TAR_{ALD}$; Bellanova et al., 2023). All event layers (E-I to E-IV) display suppressed $TAR_{ALD}$ ratios (0.43, 0.93, 1.06, and 0.95, respectively; Fig. 7) compared to the surrounding background peat and silt, ranging between 1.80 and 3.99, indicating enhanced relative contributions of short-chain *n*-aldehydes consistent with marine influence in the event deposits (Table S2).

The identified *n*-aldehyde distributions show a strong but variable even-to-odd predominance ($EOP_{ALD}$), ranging from 1.21 to 3.69 across the profile (Table S2), which generally points to the origin of cuticular waxes of higher plants, while low values (<1) would indicate input of degraded/reworked organic matter (Goodwin and Mercer, 1983; Frenken et al., 2022a). Event layers (E-I to E-IV) consistently displayed elevated $EOP_{ALD}$ values (3.5, 3.3, 3.7, and 3.2, respectively). Substantially exceeding the values of the background sediments (1.2–2.4), the event deposits are characterized by the input of fresh, unaltered plant wax aldehydes during tsunami events. Similarly, the carbon preference index for *n*-aldehydes ($CPI_{ALD}$) follows a parallel trend to the $EOP_{ALD}$,

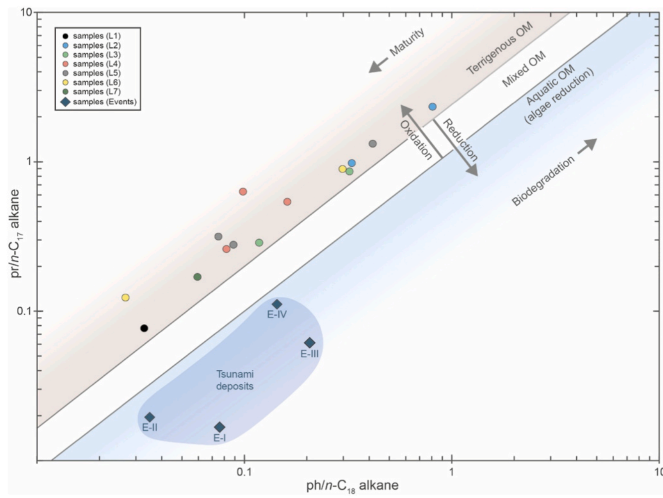


**Fig. 6.** Log-log cross-plot of isoprenoid ratios pr/$n$-$C_{17}$ to ph/$n$-$C_{18}$ indicating depositional environments and biodegradation. Background shading separates the terrigenous organic-matter (OM) field (light brown) from the aquatic organic-matter field (blue), and the intermediate band denotes mixed sources (modified after Shanmugam, 1985; Hunt, 1996). Vectors illustrate typical alteration pathways (increasing maturity, oxidation, reduction and biodegradation). Data points for event layers are displayed as blue diamonds and labeled.

with event layers exhibiting markedly elevated values (3.6–4.4) compared to background sediments (1.3–2.9), further supporting rapid deposition of fresh terrestrial organic matter during tsunami inundation.

The high-molecular-weight (HMW) *n*-aldehyde fraction, which represents the proportion of $C_{24}$–$C_{32}$ aldehydes, provides additional insights into organic matter sources. Background sediment exhibits HMW values ranging from 0.4 to 0.5, reflecting dominant terrestrial higher land plant inputs (Eglinton and Hamilton, 1967; Prahl and Pinto, 1987; Cranwell, 1991; Jetter et al., 2006). In contrast, the event layers display lower HMW values of ~0.3 (Fig. 7; Table S2), suggesting enhanced marine and/or aquatic contributions (e.g., Prahl and Pinto, 1987; Meyers, 1997, 2003). The distribution of *n*-aldehydes and their respective ratios provide a complementary dataset indicating a sudden shifts from terrigenous environments dominated by higher land plants. This reduction in the terrestrial signature within the event deposits resulted from marine incursion and the co-transport of marine algal or microbial organic matter (e.g., Meyers, 2003; Bianchi and Canuel, 2011).

#### 4.2.3. *Fatty acids*

Homologous fatty acids (FAs) from $C_{11:0}$–$C_{32:0}$ were quantified (Fig. 4). The fatty acid data (Fig. 8; Table S2) provide one of the most apparent distinctions between the event layers and background sediments. The total FA concentrations (ΣFA in μg/$g_{TOC}$) are lower in the event layers (75.4–95.7 μg/$g_{TOC}$) compared to the background sediments (109.6–195.5 μg/$g_{TOC}$), reflecting a similar pattern in compositional shifts as *n*-alkanes and *n*-aldehydes. These shifts are reflected by the distribution of short-chain ($C_{11:0}$–$C_{18:0}$) fatty acids (∑SCFA), which are typically associated with marine and aquatic microorganisms, including algae, bacteria, and phytoplankton (e.g., Meyers and Ishiwatari, 1993; Meyers, 2003). The ratio of short-chain ($C_{11:0}$–$C_{18:0}$) to long-chain ($C_{22:0}$–$C_{30:0}$) fatty acids (∑SCFA/∑LCFA) follows the same pattern as the distribution of short-chained fatty acids. Both the ∑SCFA and ∑SCFA/∑LCFA show low values (11.6–35.1 μg/$g_{TOC}$ and 0.04–0.17, respectively) in the background sediments, while they increase sharply in the event deposits (45.0–31.6 μg/$g_{TOC}$ and 0.88–3.10, respectively). All four event deposits are characterized by a dominance of short-chain fatty acids resulting from increased input of allochthonous marine organic matter during past tsunamis that inundated inland.

The ratios of LCFA/∑FA and the terrigenous-to-aquatic ratio for fatty acids ($TAR_{FA}$) show similar patterns (Fig. 8). Both the LCFA/∑FA and $TAR_{FA}$ ratios that are indicators for terrigenous environments exhibit high values (0.4–0.7 and 5.2–17.0, respectively) in the background sediments, reflecting input from higher terrestrial land plants (e.g., Eglinton and Hamilton, 1967; Eglinton and Eglinton, 2008; Alpar et al., 2012). Notably, the $TAR_{FA}$ reaches minima (0.2–1.0) in the event beds, further reinforcing the interpretation of a primary allochthonous aquatic/marine organic matter input (e.g., Meyers, 1997; Alpar et al., 2012; Konechnaya et al., 2022).

The higher plant epicuticular wax indicators, the sum of even-numbered long-chain fatty acids (∑$C_{22:0}$–$C_{32:0}$ FA) and the ∑$C_{24:0}$–$C_{32:0}$ FA/∑FA ratio, further distinguished event layers (low values of 12–28 μg/$g_{TOC}$ and 0.15–0.32, respectively) from background peat units (high values of 48–135 μg/$g_{TOC}$ and 0.47–0.76, respectively) (Fig. 8). The reduced relative proportions of terrestrial plant wax-derived fatty acids in event deposits reflect dilution by marine organic matter and/or a reduction of terrestrial inputs (e.g., Meyers, 1997; Eglinton and Eglinton, 2008; Alpar et al., 2012; Konechnaya et al., 2022). However, the presence of long-chain fatty acids in all event layers indicates terrestrial organic matter contributions, likely from erosion of coastal soils and vegetation during tsunami inundation (e.g., Richmond et al., 2012; Szczuciński et al., 2012; Bellanova et al., 2020).

The ratio of odd-chain $C_{15:0}$–$C_{17:0}$ fatty acids to total fatty acids ([$C_{15:0}$–$C_{17:0}$ FA]/∑FA) is commonly used as a bacterial (heterotrophic) lipid signal in sediments (e.g., Budge and Parrish, 1998; Gardade et al., 2021). The odd-chain FAs ($C_{15:0}$ and $C_{17:0}$) are products of bacterial metabolism (e.g., Perry et al., 1979). Generally, higher values suggest greater bacterial input, while lower values indicate dilution of short-chain fatty acids or an influx of terrestrial long-chain fatty acids (Meyers, 1997; Eglinton and Eglinton, 2008). Across the sample set, the event layers exhibited elevated ($C_{15:0}$–$C_{17:0}$ FA)/∑FA values (0.14–0.37) compared to background sediments (0.01–0.05), suggesting enhanced bacterial contributions or marine bacterial inputs associated with tsunami deposition (e.g., Asano et al., 2013, 2020; Somboonna et al., 2014; Frenken et al., 2022a; Konechnaya et al., 2022). Event layer III displays the highest value (0.37), potentially reflecting additional post-depositional microbial colonization or even greater transport of marine sediments rich in bacterial organic matter.

#### 4.2.4. *Terpenoids*

Terpenoid compounds, including monoterpenes, diterpenes, and sesquiterpenes, were analyzed as indicators of specific terrestrial plant inputs (e.g., Otto and Wilde, 2001; Peters et al., 2005; Diefendorf et al., 2014). While a diverse assemblage of terpenoid biomarkers was identified throughout the sediment core (Fig. 4), it is worth noting that not all detected diterpene and sesquiterpene peaks could be assigned to specific congeners. Furthermore, specific congeners, such as isolongifolene and longifolene, were not detected, even though they have been successfully used as indicators of organic matter from coastal pine forests (*Pinus thunbergii*) eroded by the 2011 tsunami (Shinozaki et al., 2022). The detected and quantified terpenoids include monoterpenes, diterpenes, and sesquiterpenes (Fig. 9; Table S2). These compounds, derived primarily from terrestrial vascular plants (Peters et al., 2005; Hautevelle et al., 2006) and particularly abundant in coniferous species (Otto and Wilde, 2001; Keeling and Bohlmann, 2006; Diefendorf et al., 2019), provide valuable information on the provenance of terrestrial organic matter and erosion of coastal vegetation during tsunamis (Bellanova et al., 2021; Konechnaya et al., 2022; Shinozaki et al., 2022).

Monoterpenes, volatile compounds characteristic of living plant tissues and fresh plant material, were detected in all samples with total concentrations ranging from 2400 to 16,980 ng/$g_{TOC}$ (Table S2). Background sediment units exhibit variable monoterpene concentrations (5770–16,980 ng/$g_{TOC}$), reflecting inputs from local agricultural and coastal vegetation. The lower monoterpene concentrations in event layers (E-I to E-IV; 2680, 3000, 2400, and 4940 ng/$g_{TOC}$, respectively; Fig. 9) compared to those in background peat and silt may reflect

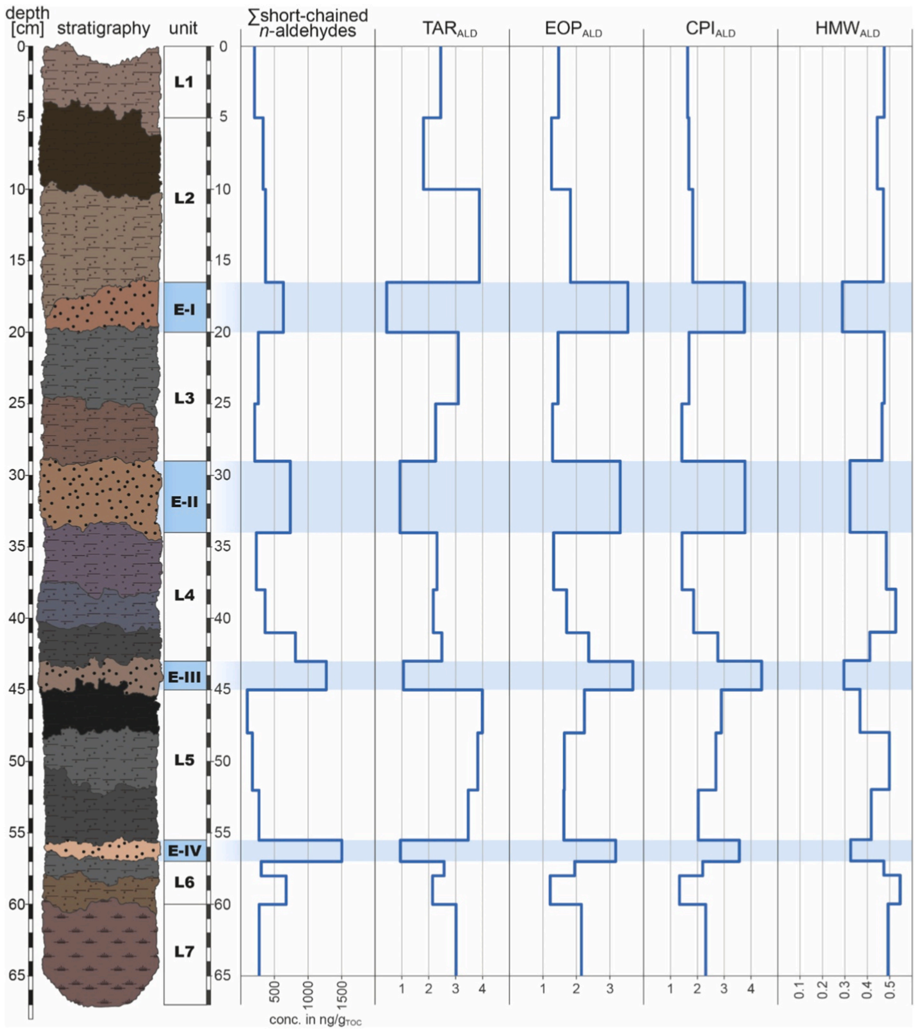


**Fig. 7.** Downcore distribution of *n*-aldehydes and their diagnostic ratios. From left to right: core stratigraphy, stratigraphic units and downcore profiles of *n*-aldehydes. Presented are the Σshort-chained ($nC_{16}$-$nC_{23}$) *n*-aldehydes (in ng/$g_{TOC}$), terrigenous-to-aquatic ratio ($TAR_{ALD}$), odd-even predominance ($EOP_{ALD}$), carbon preference index ($CPI_{ALD}$), and high-molecular-weight ratio of *n*-aldehydes ($HMW_{ALD}$). Blue shades indicate the event layers (E-I to E-IV) interpreted as tsunami deposits.

dilution by marine sediments lacking these highly volatile, plant-derived compounds due to poor sedimentary preservation (e.g., Kesselmeier and Staudt, 1999; Killops and Killops, 2013; Chetia et al., 2022).

Diterpenes, resinous compounds particularly abundant in coniferous trees (Otto and Wilde, 2001; Keeling and Bohlmann, 2006), range from 50 to 980 ng/$g_{TOC}$ across the core (Table S2). Several background sediment units exhibited elevated diterpene concentrations (240–980 ng/$g_{TOC}$), suggesting inputs from coastal pine forests lining the hills surrounding the narrow Maita River Valley (Fig. 1) and which are characteristic of the Sanriku coastline. Similar to the monoterpene distribution, the event layers (E-I to E-IV) showed reduced diterpene concentrations (70, 50, 270, and 120 ng/$g_{TOC}$, respectively). However, the diterpene signal is not as clearly suppressed as the monoterpenes. The lowest diterpene concentrations in event layers E-I and E-II may indicate limited erosion of coniferous vegetation during past marine inundations. In contrast, the moderate concentration in event layers E-III and E-IV suggests some contribution from coastal forests, soils, or potentially the destruction of pine-timber-framed housing structures.

Sesquiterpenes, intermediate molecular weight terpenoids, exhibit concentrations ranging from 250 to 1650 ng/$g_{TOC}$ throughout the profile (Table S2). Background sediments exhibit variable sesquiterpene concentrations (600–1650 ng/$g_{TOC}$), with the highest values observed in the peat units at the base of the core. Event layers (E-I to E-IV) display reduced sesquiterpene concentrations (250, 370, 510, and 370 ng/$g_{TOC}$). This suggests that the sediment transported by the tsunamis and deposited in the event beds was either marine sourced or that erosion of coastal soils and plant debris occurred. In contrast, the inter-event background sediments, particularly the peaty layers (L6 and L7), contain abundant terrestrial organic matter reflected by high TOC values. Such peaty background sediments represent a rich source of sesquiterpenes, which partially might be eroded during inundation events as seen in soil erosion during contemporary tsunamis (e.g., Richmond et al., 2012; Szczuciński et al., 2012; Bellanova et al., 2020). Generally, the sharp decrease in these plant-derived terpenoids within the event layers provides unequivocal evidence of dilution of the *in-situ* terrestrial signal by input of tsunami-derived allochthonous aquatic/marine material. In comparison, the presence and variability of terpenoid concentrations across all event layers suggest direct, but differential or limited, erosion and entrainment of coastal soils and vegetation during the four different tsunamis.

Furthermore, ratios of specific monoterpenes ([pinene + camphene + carene]/∑monoterpenes]), monoterpenes to diterpenes (monoterpene/diterpene), as well as terpenoid-generic compound ratios of cadalene and retene (e.g., [retene + cadalene]/retene or higher plant parameter – HPP; Hautevelle et al., 2006) were quantified but remained inconclusive or less indicative, only showing variations compatible with

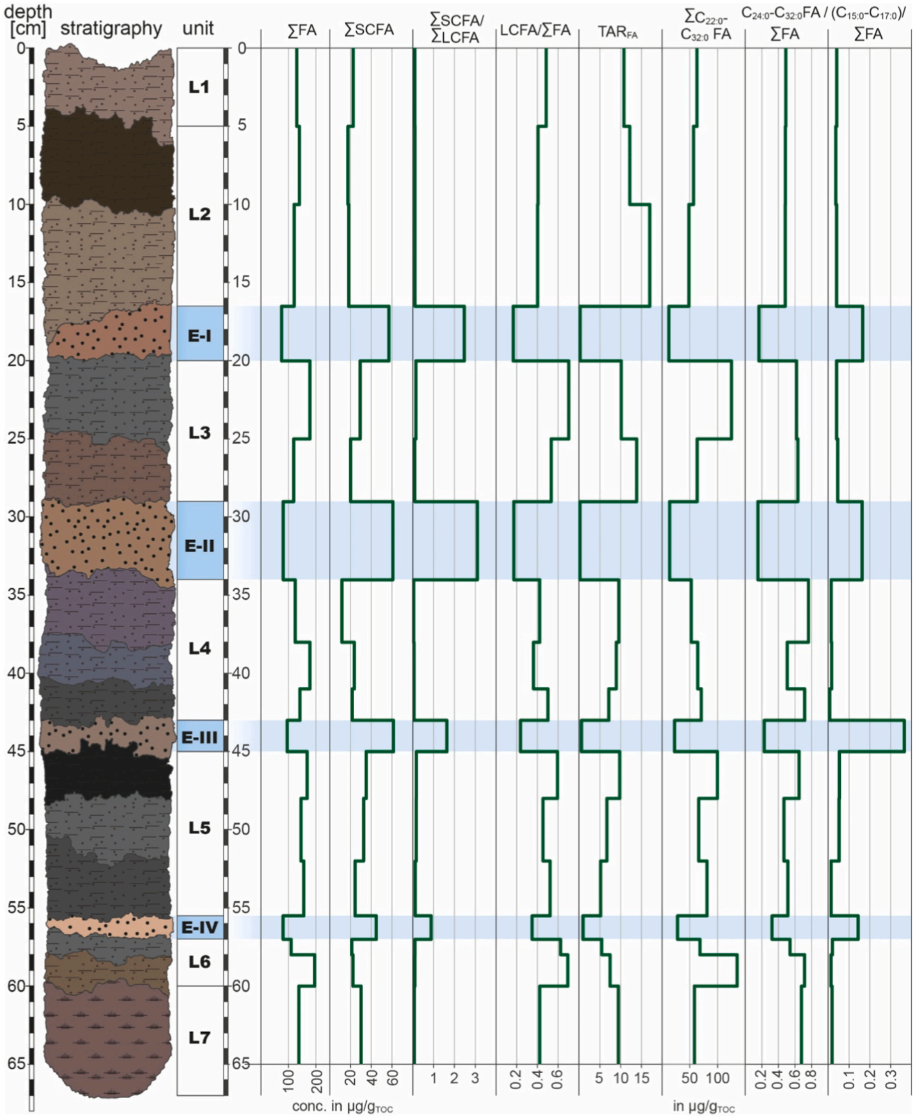


**Fig. 8.** Downcore distribution of fatty acids and their diagnostic ratios. From left to right: core stratigraphy, stratigraphic units and downcore profiles of fatty acids. Presented are concentration of total fatty acids (∑FA in µg/$g_{TOC}$), the concentration of short-chain ($C_{14:0}$-$C_{18:0}$) fatty acids (∑SCFA), the ratio of short-chain ($C_{14:0}$-$C_{18:0}$) fatty acids to long-chain ($C_{22:0}$-$C_{30:0}$) fatty acids (ΣSCFA/ΣLCFA), the ratio of long-chain ($C_{22:0}$-$C_{30:0}$) fatty acid to total fatty acids (ΣLCFA/ΣFA), the terrigenous-to-aquatic ratio of fatty acids ($TAR_{FA}$), the sum of even-numbered long-chain fatty acids (∑$C_{22:0}$-$C_{32:0}$ FA), the long-chain fatty acid to total fatty acid ratio (∑$C_{24:0}$-$C_{32:0}$ FA/∑FA), and the ratio of odd-chain $C_{15:0}$-$C_{17:0}$ fatty acids to total fatty acids ([$C_{15:0}$-$C_{17:0}$ FA]/∑FA). Blue shades indicate the event layers (E-I to E-IV) interpreted as tsunami deposits.

mobilization of coastal forest litter and resinous debris during inundation in individual event layers (e.g., Bellanova et al., 2021; Table S3). As terpenoids can be relatively volatile and reactive, they might be affected by differential degradation, thus shifting original ratios over time (Otto and Wilde, 2001; Peters et al., 2005; Killops and Killops, 2013). Therefore, terpenoids should not be used as stand-alone tsunami proxies but should be cross-referenced with biomarker proxies indicating low degradation, such as $OEP_{ALK}$ and $CPI_{ALK}$, $EOP_{ALD}$, and the pristane/$n$-$C_{17}$ versus phytane/$n$-$C_{18}$ ratio.

### 4.2.5. Hopanes and steranes

The diagenetically stable biomarkers, hopanes and steranes, which were detected throughout the sediment core (Fig. 4; Table S2), provide robust, long-term information on organic matter sources. Due to their complex cyclic molecule structure, hopanes and steranes are rarely affected by photochemical and microbial degradation (Peters and Moldowan, 1993; Suneel et al., 2014), rendering them reliable environmental indicators (Albaiges and Albrecht, 1979; Jones et al., 1986).

Hopanoids are ubiquitous molecular biomarkers occurring across diverse environments, including soils (e.g., Shunthirasingham and Simpson, 2006; Peters et al., 2005) and marine and lacustrine sediments (e.g., Ourisson et al., 1987; Peters et al., 2005; Taylor and Harvey, 2011; Doğrul Selver et al., 2015). Beyond their broad distribution, they are best known for their utility as indicators of thermal maturity in petroleum source rocks (e.g., Seifert and Moldowan, 1986; Peters et al., 2005). Petrogenic hopanoids have also been successfully used to trace destruction and remobilization associated with tsunami events (e.g., Mizukawa et al., 2017; Frenken et al., 2022b). Here, we focus on immature biohopanes ($C_{27}$–$C_{35}$), a subset derived diagenetically from bacteriohopanoid membrane lipids of diverse prokaryotes (e.g., Rohmer et al., 1984; Ourisson et al., 1987; Peters et al., 2005)), which have been detected as a suitable proxy characterizing the deposits of the 1755 CE Lisbon tsunami (Bellanova et al., 2023). The total concentration of hopanes (∑hopanes) across the samples from the Maita River Valley ranges from 0.3 to 3.8 µg/$g_{TOC}$ (Table. S2). Their concentration in background sediments, ranging from 0.3 to 1.4 µg/$g_{TOC}$, reflects

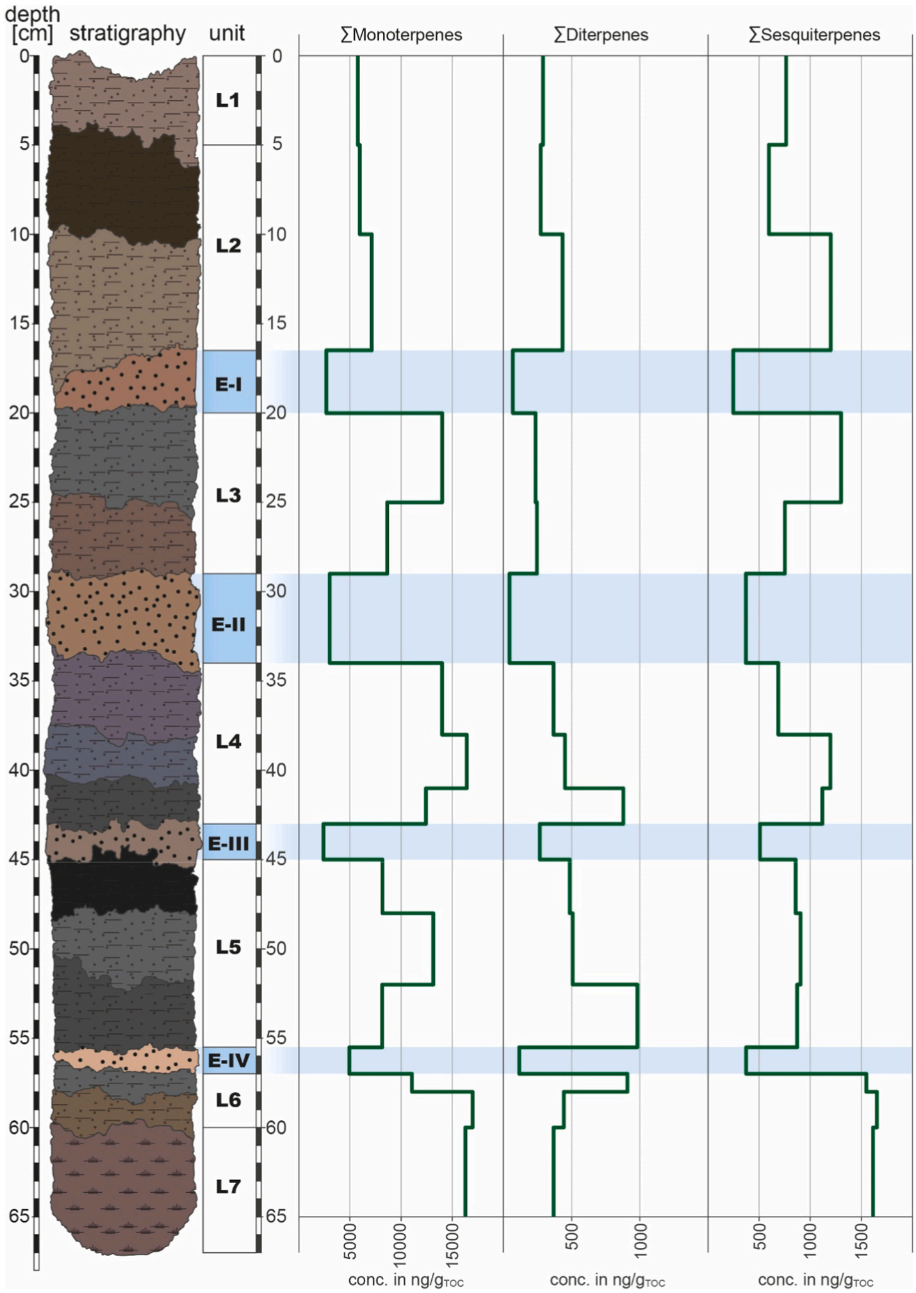


**Fig. 9.** Downcore distribution of terpenoids. From left to right: core stratigraphy, stratigraphic units and downcore profiles of terpenoids. Presented are concentration of total monoterpenes (∑monoterpenes in ng/$g_{TOC}$), concentration of total diterpenes (∑diterpenes in ng/$g_{TOC}$), concentration of total sesquiterpenes (∑sesquiterpenes in ng/$g_{TOC}$). Blue shades indicate the event layers (E-I to E-IV) interpreted as tsunami deposits.

predominantly terrestrial/soil-derived organic matter with comparatively low bacterial-lipid inputs and stronger oxidation during fluvial to estuarine deposition (Ourisson et al., 1987; Peters et al., 2005). Event layers displayed notably higher hopane concentrations ranging from 1.8 to 3.8 μg/$g_{TOC}$, which is consistent with incorporation of marine, bacterially derived organic matter (Ourisson et al., 1987) mobilized and emplaced during the high-energy inundation and backwash (e.g., Bellanova et al., 2020, 2023; Frenken et al., 2022a). The homohopane index (HHI), reflecting depositional environment characteristics and organic matter sources (ten Haven et al., 1985; Peters and Moldowan, 1991; Sinninghe Damsté et al., 1995), ranges from 0.2 to 1.8 across the profile (Table S2). Event layers (E-I to E-IV) exhibited elevated HHI values (1.3, 1.8, 1.8, and 1.1, respectively; Fig. 10), compared to the background sediments (0.2–0.9; Table S2). The interpretation of hopane isomer ratios requires caution (Peters and Moldowan, 1991; Peters et al., 2005), but the elevated values in event layers may reflect contributions of marine (Peters and Moldowan, 1991) or reworked sedimentary organic matter with different bacterial community compositions (Ourisson et al., 1987; Peters et al., 2005; Talbot and Farrimond, 2007) or may be modified during diagenetic processes (isomerization or transformation; e.g., Sinninghe Damsté et al., 1995) compared to autochthonous sediments from the Maita River Valley.

Tetracyclic steranes derive diagenetically from steroids or sterols (de Leeuw and Baas, 1986; Peters et al., 2005). In the samples, regular steranes ($C_{27}$–$C_{29}$) predominate, with a typical distribution $C_{29} > C_{28} > C_{27}$. Particularly, the $C_{27}$ steranes are reported to be indicative of marine algal and zooplanktonic sources (Huang and Meinschein, 1979; Volkman, 1986; Hudson et al., 2001) and have been associated with extreme marine incursions (e.g., Bellanova et al., 2023). The $C_{27}$ sterane concentration ranges from 110 to 1650

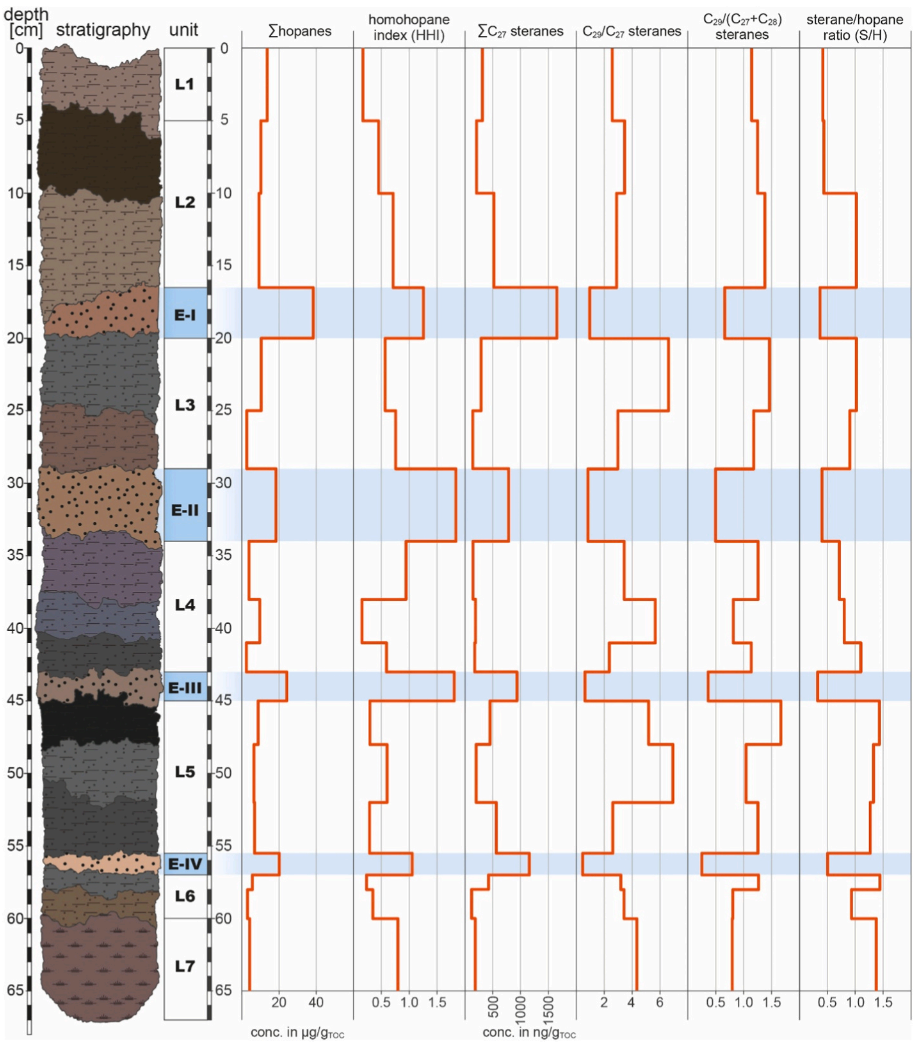


**Fig. 10.** Downcore distribution of steranes and hopanes, and their diagnostic ratios. From left to right: core stratigraphy, stratigraphic units and downcore profiles of hopanes and steranes, as well as different ratios. Presented are concentration of hopanes (Σhopanes in µg/$g_{TOC}$), the homohopane index (HHI), concentrations of $\Sigma C_{27}$ steranes (in ng/$g_{TOC}$), $C_{29}/C_{27}$ sterane ratio, $C_{29}/(C_{27}+C_{28})$ steranes ratio, and the sterane to hopane ratio (S/H). Blue shades indicate the event layers (E-I to E-IV) interpreted as tsunami deposits.

ng/$g_{TOC}$ throughout the core (Table S2). Event layers exhibited elevated $C_{27}$ sterane concentrations ranging from 780 to 1650 ng/$g_{TOC}$ compared to background sediments (110–560 ng/$g_{TOC}$; Fig. 10). In particular, event layer E-I (16.5–20 cm depth) displays the highest sterane concentration in this study (1650 ng/$g_{TOC}$), representing approximately an 8-fold enrichment relative to adjacent sediments (Fig. 10). Such significant concentration increases in the event layers provide compelling evidence for marine organic matter input, likely reflecting transport of offshore marine sediments rich in algal-derived steranes during tsunami inundation (e.g., Bellanova et al., 2023).

The $C_{29}/C_{27}$ sterane and $C_{29}/(C_{27}+C_{28})$ ratios, both distinguish terrestrial higher plant ($C_{29}$) from marine algal ($C_{27}$) and aquatic ($C_{28}$) organic matter sources (Huang and Meinschein, 1979; Volkman, 1986), providing additional discrimination between depositional environments (Table S2). Both ratios follow similar patterns (Fig. 10), with lower values reaching below unity in the event deposits compared to elevated values in the background sediments, indicating that marine-derived $C_{27}$ sterane input equals or exceeds terrestrial plant-derived $C_{29}$ sterane inputs in the event layers, providing strong evidence for substantial marine organic matter input during tsunami deposition.

This separation is visualized unequivocally in the $C_{27}$-$C_{28}$-$C_{29}$ sterane ternary plot (Fig. 11), illustrating the link between sterane proportions (in %) and depositional sources (e.g., open marine, terrestrial/land-plant, lagoonal; Huang and Meinschein, 1979; Rabbani and Kamali, 2005). The background lithologies (L1–L7) cluster in the terrestrial apex (Fig. 11), driven by $C_{29}$ sterane dominance (44.3–62.5%). The four event layers (E-I to E-IV), however, are displaced significantly towards the $C_{27}$ apex (39.9–44.3%), plotting within the open marine field (Fig. 11), providing clear evidence of their allochthonous, marine-influenced origin.

The sterane/hopane (S/H) ratio discriminates eukaryotic (algae, higher plants) from prokaryotic (bacteria) derived organic matter because steranes derive from eukaryotic sterols (Volkman, 2003; Peters et al., 2005), whereas hopanes originate from bacterial hopanoids (e.g., Ourisson et al., 1987; Peters et al., 2005). The background sediments show high S/H values (1.27–4.32), while the event units (E-I to E-IV) exhibit systematically lower values (1.1, 1.2, 1.0, and 1.5, respectively; Table S2). Elevated background signatures are consistent with terrestrial settings characterized by substantial higher sterane input from eukaryotic life and higher land plant input (Gonçalves, 2002; Sepúlveda et al., 2009). The S/H minima in the event deposits (Fig. 10) may be interpreted as a relative enrichment of hopane-bearing material during inundation, reflecting tsunami-driven erosion and the transport of microbially rich organic matter (Frenken et al., 2022a; Bellanova et al., 2023). Such S/H depressions are consistent with the use of sterane-hopane proportions to differentiate eukaryotic vs. bacterial

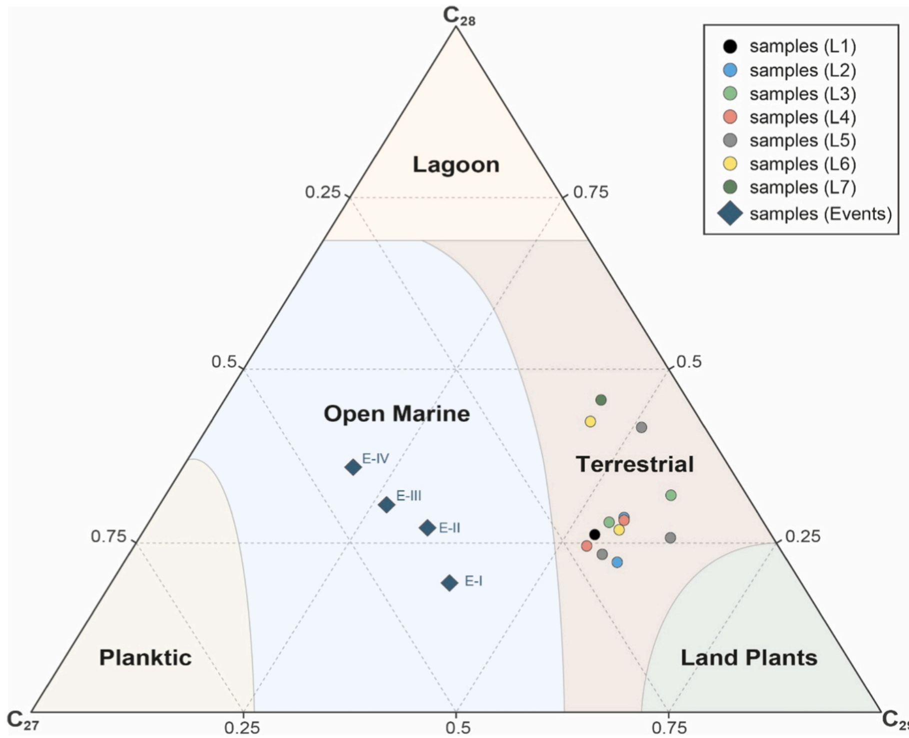


**Fig. 11.** Ternary diagram representing proportions between $C_{27}$ [%], $C_{28}$ [%] and $C_{29}$ [%] steranes. Environmental classification (planktic, open marine, lagoon, terrestrial, and land plants) are based on Huang and Meinschein (1979) and updated by Rabbani and Kamali (2005). Background units (L1-L7) are displayed as circles and event layers (E-I to E-IV) as diamonds.

inputs in sediments (e.g., Peters et al., 2005; Bobrovskiy et al., 2024).

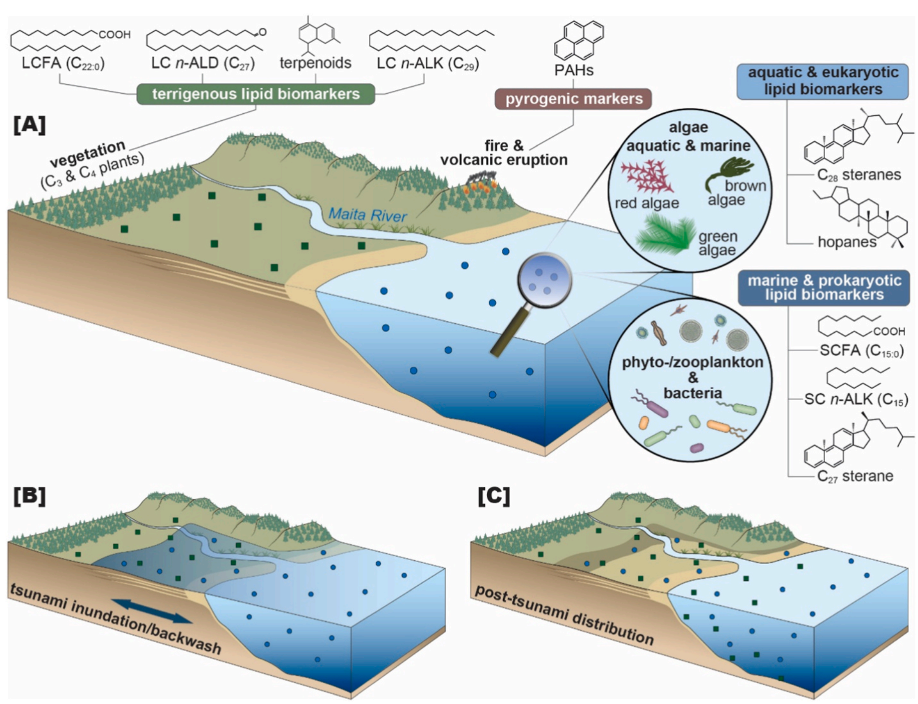


**Fig. 12.** Conceptual source-to-sink pathways of lipid biomarkers for paleotsunami detection in coastal zones. (A) Pre-event setting. Terrigenous sources from $C_3$ & $C_4$ vegetation supply long-chain fatty acids (LCFA), long-chain *n*-aldehydes (LC *n*-ALD), long-chain *n*-alkanes (LC *n*-ALK), and terpenoids (e.g., conifer resins). Wildfire and volcanism can contribute pyrogenic PAHs. Aquatic and marine sources (algae, phyto-/zooplankton, bacteria) provide short-chain fatty acids (SCFA), short-chain *n*-alkanes (SC *n*-ALK), steranes (eukaryotic), and hopanes (bacterial/prokaryotic). (B) Tsunami inundation and backwash. The tsunami entrains and mixes marine and terrestrial organic matter sources, transporting a composite of terrigenous and marine biomarkers landward and then seaward during backwash. (C) Post-tsunami distribution. Resulting deposits show landward-thinning sand sheets and muddy '*invisible*' tsunami deposits further inland.

## 5. Discussion and implications for paleotsunami research

### 5.1. Lipid biomarker as fingerprints of marine incursion by paleotsunamis

The organic geochemical analysis of the Maita sediment profile reveals distinct biomarker signatures that unequivocally differentiate the terrestrial background units (L1–L7) from the four tsunami event beds (E-I to E-IV). Sedimentologically, these event units exhibit sharp erosional bases, rip-up clasts, and some fining-upward sequences, typical of high-energy sediment transport by tsunamis. The combination with lipid biomarkers supports these findings by adding information about the source, transport and depositional processes.

#### 5.1.1. Marine vs. terrestrial signatures

The pronounced increase of short-chain *n*-alkanes ($C_{11}$–$C_{21}$) in all four event layers corroborates the influx of marine and aquatic organic matter transported landward during tsunami inundation. Specific short-chain *n*-alkanes ($C_{15}$, $C_{17}$, $C_{19}$) are ubiquitous in algae and bacteria and have been identified as marine indicators in tsunami deposits from the 2011 Tōhoku-oki event (e.g., Shinozaki et al., 2015; Bellanova et al., 2020, 2021; Frenken et al., 2022a; Konechnaya et al., 2022, Fig. 12). Short-chain *n*-aldehydes, deriving from aquatic organisms or microbial oxidation of unsaturated lipids (e.g., Prahl and Pinto, 1987; Stephanou, 1989), provide complementary evidence. The event layers exhibit pronounced peaks in short-chain *n*-aldehydes and suppressed $TAR_{ALD}$, paralleling the marine signature seen in short-chain *n*-alkanes and the corresponding $TAR_{ALK}$ ratio. The concurrent presence of long-chain *n*-alkanes and *n*-aldehydes, with high odd-over-even predominance for *n*-alkanes ($OEP_{ALK}$), even-to-odd predominance for *n*-aldehydes ($EOP_{ALD}$), and carbon preference indices ($CPI_{ALK}$, $CPI_{ALD}$) in the event layers, indicates co-transport of fresh terrestrial plant material, implying rapid burial and limited degradation during the tsunami (s). This dual signature, coupling marine input with fresh terrestrial organic matter, is characteristic of tsunami deposits where high-energy waves rapidly erode and mobilize both offshore marine sediments and coastal soil and vegetation within a single inundation and depositional pulse (e.g., Shinozaki et al., 2015, 2022; Bellanova et al., 2020, 2021). In addition, the pristane/phytane (pr/ph) ratio is a classic redox indicator (Didyk et al., 1978; Ten Haven et al., 1987; Powell, 1988) with values $< 0.8$ reflecting reducing, often marine depositional environments (e.g., Powell, 1988; Peters et al., 2005), whereas values $> 3$ indicate oxic conditions and terrestrial plant input (e.g., Ten Haven et al., 1988). All four event layers consistently show pr/ph ratios $<0.7$, a signature commonly associated with organic matter derived from reduced or anoxic marine bottom waters or resuspended seafloor sediments (e.g., Didyk et al., 1978) and may further reflect potential contribution from phytoplanktonic chlorophyll degradation (e.g., Rontani and Bonin, 2011). Although tsunami waters are oxygenated at the wave surface, tsunamis can entrain and redeposit reduced marine sediments and associated organic matter (e.g., Ikehara et al., 2021), and rapid burial can limit re-oxygenation and favor reducing conditions within the tsunami deposit (e.g., Watanabe et al., 2020), consistent with the observed low pr/ph ratios. By contrast, background sediments have higher pr/ph values in combination with long-chain *n*-alkanes, indicating a stronger terrestrial plant-wax input and comparatively more oxic to redox-variable conditions (e.g., Eglinton and Hamilton, 1967; Meyers, 2003) common in aerated near-surface soils (e.g., cultivated soils; e.g., Maruoka et al., 2015) or exposure prior to burial, rather than permanently waterlogged peat, which is generally reducing (e.g., Chagué-Goff, 2010; Watanabe et al., 2020).

Notably, the consistent marine biomarker signature documented across all four event layers (E-I to E-IV) contrasts with the absence of marine bioclasts from these deposits. This dissociation is not unexpected, as the organic-rich, acidic peat and silt units surrounding the event deposits within the Maita River Valley's stratigraphy promote dissolution of calcareous tests and shell fragments over long periods of time, as reported elsewhere (e.g., Chagué-Goff et al., 2012; Szczuciński, 2020; Hawkes, 2020; Putra et al., 2023). Yet, this observation illustrates a key strength of lipid biomarkers relative to conventional bioclast-based proxies in such settings. Organic compounds sourced from marine algae, phytoplankton, and marine bioclasts, such as shells or foraminifera, can survive in the sediment-geochemical record and document marine inundations, even where all macro- and microscopic calcareous evidence may have been destroyed by diagenetic dissolution. In this sense, the marine lipid biomarker signal constitutes a complementary proxy, partially compensating for the loss of marine bioclasts.

The hopanes and sterane distributions provide particularly robust evidence for marine influence. Marine $C_{27}$ steranes (algae and zooplankton) and the $C_{29}/C_{27}$ sterane ratio (terrestrial vs. marine organic matter input), homohopane index (HHI, marine bacterial contribution), and sterane/hopane ratio (S/H, eukaryotic vs. prokaryotic ratio) all indicate marine sources dominating the organic matter composition of the event layers. Particularly useful is the ternary plot of the percentual distribution of steranes ($C_{27}$, $C_{28}$, $C_{29}$) (Fig. 11; Fig. 12), which clearly distinguishes the four event deposits as marine sourced. This observation aligns with recent findings by Bellanova et al. (2023), who demonstrated that steranes and hopanes can preserve source information for historic tsunami events, such as the 1755 CE Lisbon tsunami.

The dilution or depletion of distinct terrigenous biomarker proxies further elucidates source contributions of the four event deposits. Particularly long-chain homologues of *n*-alkanes ($C_{25}$–$C_{35}$), *n*-aldehydes ($C_{26}$–$C_{32}$, fatty acids ($C_{22:0}$–$C_{30:0}$), and terpenoids (mono-, di-, and sesquiterpenes) are (volatile) plant metabolites that can signal the input of higher plant waxes and specific vegetation types (Eglinton and Hamilton, 1967; Otto and Wilde, 2001). These characteristics are consistent with terrestrial soil accumulation (e.g., Otto and Wilde, 2001; Meyers, 2003; Bellanova et al., 2021; Shinozaki et al., 2022). The event layers, however, show a sharp decline in terrigenous input, as indicated by low diterpene and sesquiterpene concentrations, low LCFA/ΣFA and $TAR_{FA}$ ratios, and high ΣSCFA/ΣLCFA values (e.g., Bourbonniere and Meyers, 1996; Konechnaya et al., 2022; Shinozaki et al., 2022). Reflecting this, are short-chain ($C_{14:0}$–$C_{18:0}$) fatty acids or the $C_{15:0}$–$C_{17:0}$ FA)/$\sum$FA ratio, which clearly suggest marine sourced organic matter being present only in the four event deposits. Furthermore, elevated odd-chain bacterial fatty acids (e.g., $C_{15:0}$–$C_{17:0}$) in event layers indicate bacterial input or growth after deposition, perhaps reflecting selective microbial colonization of tsunami deposits (event fauna – Asano et al., 2013, 2020; Hiraoka et al., 2016). Combined, the declining terrigenous proxy patterns imply an influx of marine organic matter (Alpar et al., 2012; Shinozaki et al., 2015; Konechnaya et al., 2022) and dilution of terrestrial matter, which may be eroded and entrained during inundation, thus tracing erosion pathways and sediment provenance (e.g., Bellanova et al., 2020; Frenken et al., 2022a; Shinozaki et al., 2022).

#### 5.1.2. Biomarker potential for detecting 'invisible' tsunami deposits

Detection of silty and muddy tsunami deposits on top of or blending into soil stratigraphies beyond the limit of sand, sometimes referred to as '*invisible*' deposits, remains challenging even for contemporary events (e.g., Goto et al., 2011; Richmond et al., 2012; Chagué-Goff et al., 2012; Szczuciński et al., 2012; Bellanova et al., 2021; Shinozaki et al., 2022). It has also only been rarely demonstrated for historical or paleotsunami deposits (Moreira et al., 2017; Chagué et al., 2020; Komeiji et al., 2025). However, organic markers present a potential proxy capable of detecting such '*invisible*' tsunami deposits (e.g., Bellanova et al., 2021; Shinozaki et al., 2022; Komeiji et al., 2025) and therefore may be a valuable tool to extend reconstructions of inundation distances in paleotsunami studies.

The results of this case study illustrate how lipid biomarker proxies may also capture ('*invisible*') tsunami mud. Several marine-terrestrial ratios show a stepwise, rather than instantaneous, recovery above the sandy event beds (at 25–34 cm and 40–45 cm, respectively; e.g., $TAR_{ALK}$

– Fig. 5; $TAR_{ALD}$, $CPI_{ALD}$ – Fig. 7; $TAR_{FA}$, LCFA/∑FA – Fig. 8; $C_{29}/C_{27}$ steranes – Fig. 10). Such observations are consistent with the few descriptions of tsunami muds studied beyond sand limits (e.g., Chagué-Goff et al., 2012; Bellanova et al., 2021; Shinozaki et al., 2022; Komeiji et al., 2025). However, it needs to be noted that our sampling strategy and resulting vertical resolution was not targeted to and thus does not allow a definitive analysis and distinction of the potential '*invisible*' fraction of the tsunami deposits in the Maita River Valley. Nonetheless, this shall motivate future high-resolution sampling and targeted approaches across lateral transects beyond the sand limit to test biomarker detectability of the muddy '*invisible*' tsunami deposits.

#### *5.1.3. Comparison with modern tsunami deposits and other studies*

The detected lipid biomarker patterns from the sediment profile in the Maita River Valley exhibit remarkable consistency with findings from modern tsunamis, particularly they agree with previous observations of the well-studied 2011 Tōhoku-oki tsunami (Table 1; e.g., Shinozaki et al., 2015, 2016; Bellanova et al., 2020, 2021; Frenken et al., 2022a; Konechnaya et al., 2022; Komeiji et al., 2025). The results confirm that biomarkers and diagnostic ratios which previously have been applied on modern deposits, such as *n*-alkanes, isoprenoids, steranes, hopanes, *n*-aldehydes, and fatty acid distributions, effectively discriminate paleo-tsunami sediments from background sediments. The congruence between modern analogues and the presented paleotsunami results validates the temporal robustness of organic geochemical proxies and supports their application to ancient event deposits.

The non-detection (concentrations $<$ LOQ) or absence of specific lipid biomarkers in an event deposit is circumstantial and does not refute the environmental and process information value of the detected compounds. Specific singular compounds with high source specificity (e.g., isolongifolene, dinosterol; Shinozaki et al., 2022) may be absent from deposits, as their presence depends on the local occurrence of their biological producers, specific sources, and tsunami hydraulics to entrain, transport, and deposit them. Therefore, their absence records source or taphonomic constraints, rather than indicating that extreme inundation events did not occur. In the example of the Maita River Valley, with an open estuarine setting with coniferous vegetation on the hillsides but only agricultural or fluvial vegetation in the valley, the incorporation of isolongifolene into the studied tsunami deposits was not directly expected. This stands in contrast to settings, such as the Sendai Plain, where a coastal coniferous forest separates the coastline from the inland areas, and the 2011 Tōhoku-oki tsunami flow travelled inland across the forest. In such local circumstances, the entrainment and preservation of environment specific biomarkers, such as isolongifolene, serve as exceptionally well-suited markers to trace tsunami inundation beyond the limit of sand (e.g., Shinozaki et al., 2022).

Overall, the need for multi-proxy approaches was highlighted by Chagué-Goff et al. (2011, 2017) and Bellanova et al. (2019), with the latter two studies argued that organic geochemical proxies in particular generally provide high source specificity and environmental information, complementing sedimentological and other geochemical tsunami indicators. The results of this study validate this claim, as findings across multiple independent compound classes represent one of the first comprehensive applications of lipid biomarkers to paleotsunami deposits and demonstrate their utility and viability as diagnostic tools for identifying marine incursions in the sedimentary record, thereby providing a reliable signal for paleotsunami deposits.

### *5.2. Limitations and future perspectives*

#### *5.2.1. Preservation of organic signatures*

Despite the promising results, several limitations warrant careful consideration. Aside from site context and source-specific limitations, grain size effects, differential preservation and diagenesis are primary concerns when applying organic geochemical proxies to ancient tsunami deposits. Preferential adsorption of biomarkers onto fine, organic-rich particles and matrix effects can modulate detectability, and prior work debated whether missing marine signals reflect non-transport or post-depositional loss (e.g., Shinozaki et al., 2015, 2016; Shinozaki, 2021). In coastal forests, short-chain *n*-alkanes and other marine biomarkers may be absent from sandy deposits because they bind to fine sediments that settle into mud caps rather than sandy deposits (Shinozaki et al., 2015, 2022). Thus, site-specific factors (e.g., vegetation, hydrodynamics, sediment supply) can control biomarker preservation (e.g., Shinozaki et al., 2016, 2022; Chagué, 2020; Shinozaki, 2021; Frenken et al., 2022a; Chagué and Shinozaki, 2023). Nonetheless, multiple studies show that sandy tsunami deposits can retain diagnostic lipids, especially when employing multiple biomarker classes and ratios, and integrating stratigraphic and site-specific context (e.g., Bellanova et al., 2020, 2023; Shinozaki et al., 2022), misinterpretations can be minimized. For instance, Frenken et al. (2022a) cautioned that $TAR_{ALK}$ values must be interpreted in the context of local source materials because tsunami deposits contain mixtures of eroded marine and terrestrial sediments. Normalizing biomarker concentrations to total organic carbon (TOC) content mitigates the influence of variable organic matter abundance across stratigraphic units and allows for more meaningful comparisons between event and background strata (e.g., Frenken et al., 2022a; Konechnaya et al., 2022). This normalization is essential in paleotsunami contexts where sandy event layers typically exhibit lower TOC (~3–5%) than organic-rich background soils or peats (~8–24%). The clear separation of event and background signatures, even after TOC normalization, confirms that the observed biomarker patterns reflect true compositional differences in organic matter sources rather than mere grain-size effects (Frenken et al., 2022a). The grain size contrast between the fine-grained units (L) and the sandy event units (E) is relevant from an organic geochemical perspective, as fine particles possess greater specific surface area and thus higher organic matter adsorption capacity, resulting in inherently higher absolute biomarker concentrations in the background units independently of source differences (e.g., Keil and Hedges, 1993; Frenken et al., 2022a). Frenken et al. (2022a) have shown that TOC normalization effectively corrects for this grain-size-driven dilution effect and outperforms normalization over the fine grain fraction in tsunami-related biomarker studies. Although marine-sourced biomarkers preferentially adsorb onto finer particles rather than coarse sandy deposits (Shinozaki et al., 2015, 2022), the robust marine fingerprint consistently detected across all four event layers after TOC normalization confirms that marine organic matter is significantly retained within the sandy event units (E) to yield a reliable and interpretable proxy signal comparable to previous studies (e.g., Bellanova et al., 2020, 2021, 2023; Frenken et al., 2022a). Notably, the event layers are not composed of pure sand, as mud content ranges from 0 to 3% and silt content from 9 to 18% across the four units (Table S1), a non-negligible fine-grained fraction that may itself contribute to biomarker adsorption and preservation within these otherwise sand-dominated layers.

Yet, biomarker preservation may be influenced by compound volatility, biodegradation, and sediment reworking. Labile compounds such as sterols, terpenoids, and polyunsaturated fatty acids are susceptible to microbial degradation (e.g., Keil and Hedges, 1993; Burdige, 2007), oxidation (e.g., Rontani, 2001; Marchand and Rontani, 2001; Rontani et al., 2007), and thermal alteration (e.g., Peters et al., 2005; Killops and Killops, 2013), potentially erasing or distorting source signatures (Shinozaki et al., 2016; Chagué-Goff et al., 2017). This may be the reason why alkenones were not detected in this study; however, their absence more likely reflects a limited contribution from their haptophyte algal source than post-depositional degradation, consistent with the general scarcity of alkenones reported in tsunami deposits (e.g., Rontani et al., 2013; Shinozaki et al., 2015, 2016). Likewise, certain terpenes can degrade rapidly (e.g., van Roon et al., 2005a, 2005b; Marmulla and Harder, 2014) despite the presence of coastal vegetation. Consequently, terpenoids should not be used as stand-alone proxies, and their low concentration in the event layers of the Maita River Valley may reflect degradation rather than the absence of terrestrial vegetation. However, for this study cross-verification with more stable compounds (e.g., *n*-alkanes and hopanes), and the $OEP_{ALK}$ and $EOP_{ALD}$ ratios, suggests the deposition of fresh material and limited postdepositional degradation (Prahl and Pinto, 1987; Thomas et al., 2021; Frenken et al., 2022a).

A key observation in the context of this case study from the Maita River Valley is that biomarker preservation is broadly comparable across all four event layers (Inoue et al., 2017; Ishizawa et al., 2022). This is evident, particularly for the most diagenetically stable compound classes, including *n*-alkanes, steranes, and hopanes (Fig. 5; 10), confirming that lipid biomarkers, once embedded in the organic-rich peat or silt matrix, can be preserved on millennial timescales, when local environmental conditions suppress microbial degradation and oxidation (e.g., Meyers, 2003; Peters et al., 2005; Burdige, 2007). However, compound-class-specific hierarchies of preservation and diagenetic sequences have been documented in organic-rich sediments (e.g., Cranwell, 1981; Meyers and Ishiwatari, 1993; Canuel and Martens, 1996; Wakeham et al., 1997). This is consistent with the observed absence of less stable organic compounds in this case study. Critically, the marine biomarker fingerprint remains detectable and interpretable in all four event layers, even if marine bioclasts are absent or have dissolved over time, confirming that biomarkers provide a robust proxy for paleotsunami reconstruction in coastal sedimentary archives.

#### 5.2.2. Multi-compound approach and future perspectives

Given the possible limitations, future research should include systematic multi-compound analyses of biomarkers as presented in this case study, as well as continuously review utilizable lipid proxies to gain further insights into paleotsunami preservation potential as a function of deposit age, lithology, and burial history. The integration with complementary proxies can further support the robustness of paleotsunami identification. Additional biomarker proxies that could be useful but have not been detected and tested in this study include glycerol dialkyl glycerol tetraether lipids (GDGTs), such as crenarchaeol and branched GDGTs, using the branched and isoprenoid tetraether (BIT) index to assess marine versus terrestrial input (e.g., Hopmans et al., 2004; Schouten et al., 2013) and their respective ratios. Moreover, long-chain *n*-alcohols or wax esters, and the pyrolysis of lignin phenols (e.g., Konechnaya et al., 2022) may also represent promising additions to the known biomarker-set for paleotsunami research. Furthermore, integrating other organic geochemical analyses can provide a broader picture, such as compound-specific isotope analysis (CSIA). Such analyses represent promising but underutilized techniques in tsunami research (e.g., Chagué-Goff et al., 2017; Shinozaki, 2021). CSIA on *n*-alkanes, fatty acids, or amino acids can provide additional source discrimination by isotopically fingerprinting terrestrial material ($C_3$ vs. $C_4$ plants) and contrasting them to marine organic matter (e.g., Alewell et al., 2016; Hirave et al., 2020). Integrating CSIA with lipid biomarker distributions could enhance source allocation and improve confidence in paleotsunami identification, particularly in settings where multiple organic matter sources overlap.

Likewise, the utilization of environmental DNA has proven to be a powerful analytical tool in paleotsunami research (e.g., Szczuciński et al., 2016; Engel et al., 2020; Yap et al., 2021, 2023; Shinozaki et al., 2025), and while it is increasingly used, it is still not widely adopted across tsunami studies. Coupling lipid biomarkers with eDNA analysis can provide high taxonomic resolution of marine organisms (e.g., diatoms, foraminifera) preserved in tsunami deposits (e.g., Shinozaki et al., 2025) and provide further evidence to differentiate tsunami deposits from the background or distinguish them from other extreme events, such as storms (Somboonna et al., 2014; Switzer et al., 2016; Szczuciński et al., 2016; Yap et al., 2021). Storm waves typically mobilize sediment from narrower coastal source areas, primarily beach and dune material, with limited entrainment of shallow offshore sediment (e.g., Morton and Sallenger Jr, 2003; Morton et al., 2007; Watanabe et al., 2021). Tsunami inundation, by contrast, transports organic matter from a much wider range of marine source environments, including offshore phytoplankton, reduced seafloor sediments, and marine-derived organic matter transported far inland (e.g., Shinozaki et al., 2015; Bellanova et al., 2020, 2023; Konechnaya et al., 2022). These differences in sediment and organic matter source areas may produce distinct variations in the biomarker signatures. Particularly, short-chain *n*-alkanes, pr/ph ratios, and marine steranes could be useful biomarker proxies potentially indicating lower values in storm deposits compared to tsunami event layers. If confirmed through targeted comparative studies, specific lipid biomarker criteria could emerge as independent proxies for discriminating between tsunami and storm deposits, addressing a longstanding challenge in tsunami research (e.g., Morton et al., 2007; Goff et al., 2012; Goto et al., 2015).

Finally, the spatial resolution and lateral continuity of biomarker signatures, as well as the baseline variability in local organic matter (e.g., vegetation changes, land-use changes), must be better constrained through future research. Modern examples show that biomarker proxies can successfully trace the extent of inland inundation; however, for paleotsunamis, this knowledge is limited. The four analyzed event layers from Maita show consistent biomarker patterns at the single coring location. Additional cores across the river valley, and neighboring sites (e.g., Noda) are needed to assess spatial variability and confirm that biomarker signatures can trace paleotsunami deposits inland and identify inland inundation beyond the limit of visually recognizable sand deposits.

### 5.3. Methodological implications for paleotsunami research

The Sanriku coastline represents a region with a long paleotsunami history linked to its high seismic activity and vulnerability to subduction-zone tsunamis (Fig. 1). However, compared to the Sendai and Ishinomaki Plains, paleotsunami research on the Sanriku coast has received less attention, partly due to the challenging geomorphology with narrow valleys, limited coastal lowlands, and steeply incised ria coastlines that reduce sedimentary preservation potential (e.g., Naruse et al., 2012; Yamada et al., 2014; Goto et al., 2015, 2019; Inoue et al., 2017; Yokoyama et al., 2021; Ishizawa et al., 2022). Previous studies have identified up to 12–14 historical and prehistoric tsunamis over the past 4000 years along this coastline, with recurrence intervals estimated between 350 and 600 years (e.g., Ishimura and Miyauchi, 2015; Sawai et al., 2015; Inoue et al., 2017; Ishimura, 2017; Ishizawa et al., 2022).

The primary contribution of this study to paleotsunami research is of methodological nature. Biomarker proxies had been individually applied to modern tsunami deposits (primarily the 2011 tsunami deposits, e.g., Shinozaki et al., 2015, 2016, 2022; Bellanova et al., 2020, 2021; Konechnaya et al., 2022) and in a few cases on historical tsunami deposits (e.g., Alpar et al., 2012; Mathes-Schmidt et al., 2013; Bellanova et al., 2023; Komeiji et al., 2025); however, they have never been systematically applied to paleotsunami deposits. Through the review of suitable paleotsunami biomarker proxies and by applying them for the first time in a multi-compound approach to paleotsunami deposits, this study demonstrates that this approach can independently fingerprint marine inundation events. It further corroborates tsunami interpretations on sediment sources, organic-matter provenance, redox conditions, and transport processes over millennial timescales. The added value of the Maita River Valley case study lies in the confirmation and characterization of the four previously described and chronologically constrained event layers (Inoue et al., 2017; Ishizawa et al., 2022) through robust multi-proxy biomarker signals, as a controlled test case in which the biomarker approach can be evaluated against an independently established paleotsunami stratigraphy. Furthermore, the successful application of lipid biomarkers to the Maita River Valley deposits confirms that biomarker preservation is sufficient for paleotsunami research. It also shows that organic geochemistry can offer a complementary approach to strengthen paleotsunami interpretations, reliably reconstruct paleotsunami magnitudes, possibly revealing their inundation extent beyond the visible sand deposits, and discriminating sediment sources and transport processes and pathways. These resulting methodological implications are transferable beyond the Japanese Sanriku coast. In geomorphologically challenging settings with limited coastal lowlands, and reduced sedimentary preservation potential, where sand sheets are discontinuous or visually ambiguous, or where bioclast preservation is poor, lipid biomarkers may help identify or discriminate marine-inundation deposits from terrestrial background sediment. For the Sanriku coast specifically, this approach complements existing paleotsunami chronologies, and thus this has important implications for seismic hazard assessment, as paleoseismic data inform probabilistic models of future tsunami risk (e.g., Annaka et al., 2007; Goto et al., 2011; Namegaya and Satake, 2014; Sawai et al., 2015; Ishimura, 2017).

## 6. Conclusions

This study presents a review of lipid biomarkers suitable as paleotsunami proxies and their first comprehensive application to paleotsunami deposits on the Sanriku coast (Japan). The Sanriku coast is characterized by challenging geomorphological conditions and limited sedimentary archives, underscoring that organic geochemistry offers robust, source-specific, and complementary tools to traditional sedimentological methods in tsunami research for identifying and characterizing marine incursions over millennial timescales. The combined sedimentological systematic lipid biomarker analysis of the sediment profile from the Maita River Valley reveals four distinct sand beds (E-I to E-IV). These results demonstrate that tsunami event layers can be detected and characterized without requiring tightly constrained age models, while highlighting that comparison with previously documented chronologies can provide tentative age constrains, suggesting a tsunami record comprising four paleotsunami events, including a possible correlation with the 869 CE Jōgan tsunami and three older paleotsunamis. Each event layer exhibits diagnostic geochemical fingerprints collectively indicating (1) increased marine proxies, such as elevated short-chain homologues (*n*-alkanes, *n*-aldehydes, fatty acids), enriched $C_{27}$ steranes, and higher $C_{15:0}$–$C_{17:0}$ FA)/$\sum$FA, (2) reduced plant-derived terrestrial signatures, such as terrigenous-to-aquatic ratios ($TAR_{ALK}$, $TAR_{ALD}$, $TAR_{FA}$), long-chain homologues (*n*-alkanes, *n*-aldehydes, fatty acids), terpenoids, $C_{29}/C_{27}$ sterane ratio, and (3) distinctive prokaryotic over eukaryotic signatures from sterane/hopane (S/H) distributions or the homohopane index.

Both marine- and terrigenous-derived biomarkers have diagnostic values when interpreted in context (Fig. 12). Combining these markers allows to unequivocally differentiate the tsunami sand beds from the terrestrial background silty units (L1–L7). As environmental and process indicators, biomarkers provide information on entrainment, transport, and deposition of marine-sourced particle-bound organic matter typical of such marine incursions.

A critical strength lies in comprehensive multi-compound approaches, providing robust indicators and proxies, ensuring that marine signatures can be detected even when individual biomarker classes are compromised by degradation or differential preservation. These findings align with and extend previous biomarker studies on modern tsunami deposits, validating the temporal applicability of organic geochemical fingerprinting across historic and prehistoric events.

Overall, this work highlights the analytical value of organic geochemistry in paleotsunami research. By identifying coherent biomarker signatures associated with tsunami deposition, we provide a framework for future studies to detect and characterize prehistoric tsunamis in a variety of coastal depositional settings.

## Author contributions

P.B., J.S., and K.R. conceptualized the research design of this review and case study. J.S., K.R., and P.B. were responsible for funding acquisition. P.B. was involved in all aspects of this research, including planning and conducting all aspects of the research, data curation, and analytical work. Y.N., J.S., and P.B. executed the field survey. P.B. executed the grain-size analysis and organic geochemical analyses. P.B., J.S., and T.S. conducted the geochemical interpretations. P.B., Y.N., D. S., T.S., C.C., K.R., and J.S. guided the intellectual direction of this research paper. P.B. wrote and visualized the original draft, and all authors reviewed and edited the manuscript.

## Declaration of competing interest

The authors declare that they have no known competing financial interests or personal relationships that could have appeared to influence the work reported in this paper.

## Acknowledgments

This study was supported financially by the German Research Foundation (DFG) 390538253. We thank Yvonne Esser and Denis Jarmulkowicz for their support during sample processing and Annette Schneiderwind for her technical support during GC-MS analysis. We also thank the landowner for granting access to the field site. Finally, we would like to thank Dr. R. Paris and an anonymous reviewer for their constructive comments and suggestions, which helped improve this article significantly.

## Appendix A. Supplementary data

Supplementary data to this article can be found online at https://doi.org/10.1016/j.quascirev.2026.110188.

## Data availability

All data and/or code is contained within the submission.

## References

Abe, T., Goto, K., Sugawara, D., 2020. Spatial distribution and sources of tsunami deposits in a narrow valley setting – insight from 2011 Tohoku-oki tsunami deposits in northeastern Japan. Prog. Earth Planet. Sci. 7, 7. https://doi.org/10.1186/s40645-019-0318-6.

Albaiges, J., Albrecht, P., 1979. Fingerprinting marine pollutant hydrocarbons by computerized gas chromatography-mass spectrometry. Int. J. Environ. Anal. Chem. 6, 171–190. https://doi.org/10.1080/03067317908071170.

Alewell, C., Meusburger, K., Brodbeck, M., Bänninger, D., 2016. Quantitative sediment source attribution with compound-specific isotope analysis in a C3 plant-dominated catchment. Biogeosciences 13, 1587–1605. https://doi.org/10.5194/bg-13-1587-2016.

Alpar, B., Ünlü, S., Altınok, Y., Özer, N., Aksu, A., 2012. New approaches in assessment of tsunami deposits in dalaman (SW Turkey). Nat. Hazards 63, 181–195. https://doi.org/10.1007/s11069-010-9692-5.

Annaka, T., Satake, K., Sakakiyama, T., Yanagisawa, K., Shuto, N., 2007. Logic-tree approach for probabilistic tsunami hazard analysis and its applications to the Japanese coasts. Pure Appl. Geophys. 164, 577–592. https://doi.org/10.1007/s00024-006-0174-3.

Asano, R., Hayakawa, A., Fukushima, J., Nakai, Y., Shimura, Y., Abe, M., Inamoto, T., 2020. Changes in bacterial communities in seawater-flooded soil in the four years after the 2011 tohoku tsunami in Japan. J. Mar. Sci. Eng. 8, 76. https://doi.org/10.3390/jmse8020076.

Asano, R., Nakai, Y., Kawada, W., Shimura, Y., Inamoto, T., Fukushima, J., 2013. Seawater inundation from the 2011 tohoku tsunami continues to strongly affect soil bacterial communities 1 year later. Microb. Ecol. 66, 639–646. https://doi.org/10.1007/s00248-013-0261-9.

Bellanova, P., Feist, L., Mathes-Schmidt, M., Frenken, M., Schwarzbauer, J., Reicherter, K., 2023. Small-scaled variations in the 1755 CE tsunami deposits – observations from a sedimentological trench. Cont. Shelf Res. 267, 105097. https://doi.org/10.1016/j.csr.2023.105097.

Bellanova, P., Frenken, M., Nishimura, Y., Schwarzbauer, J., Reicherter, K., 2021. Tracing woody-organic tsunami deposits of the 2011 Tohoku-oki event in Misawa (Japan). Sci. Rep. 11, 8947. https://doi.org/10.1038/s41598-021-88199-3.

Bellanova, P., Frenken, M., Reicherter, K., Jaffe, B., Szczuciński, W., Schwarzbauer, J., 2020. Anthropogenic pollutants and biomarkers for the identification of 2011

Tohoku-oki tsunami deposits (Japan). Mar. Geol. 422, 106117. https://doi.org/10.1016/j.margeo.2020.106117.
Bellanova, P., Frenken, M., Richmond, B., Schwarzbauer, J., La Selle, S., Griswold, F., Jaffe, B., Nelson, A., Reicherter, K., 2019. Organic geochemical investigation of far-field tsunami deposits of the Kahana valley. O'ahu, Hawai'i. Sedimentol 67, 1230–1248. https://doi.org/10.1111/sed.12583.
Bellanova, P., Schwarzbauer, J., Reicherter, K., 2024. Inventory of aqueous and sediment-associated organic pollutants released by the 2021 flood in the vicht–Inde catchment, Germany. Environ. Sci. Eur. 36, 110. https://doi.org/10.1186/s12302-024-00925-6.
Bernard, E., 2012. Tsunamis: are we underestimating the risk? Oceanogr. 25, 208–218. https://doi.org/10.5670/oceanog.2012.60.
Bianchi, T.S., Canuel, E.A., 2011. Chemical Biomarkers in Aquatic Ecosystems. Princeton University Press, Princeton, NJ.
Blott, S.J., Pye, K., 2001. GRADISTAT: a grain size distribution and statistics package for the analysis of unconsolidated sediments. Earth Surf. Proc. Landf. 26, 1237–1248. https://doi.org/10.1002/esp.261.
Bobrovskiy, I., Poulton, S.W., Hope, J.M., Brocks, J.J., 2024. Impact of aerobic reworking of biomass on steroid and hopanoid biomarker parameters recording ecological conditions and thermal maturity. Geochem. Cosmochim. Acta 364, 114–128. https://doi.org/10.1016/j.gca.2023.11.024.
Bourbonniere, R.A., Meyers, P.A., 1996. Sedimentary geolipid records of historical changes in the watersheds and productivities of Lakes Ontario and Erie. Limnol. Oceanogr. 41, 352–359. https://doi.org/10.4319/lo.1996.41.2.0352.
Budge, S.M., Parrish, C.C., 1998. Lipid biogeochemistry of plankton, settling matter and sediments in Trinity Bay, Newfoundland. II. Fatty acids. Org. Geochem. 29, 1547–1559. https://doi.org/10.1016/S0146-6380(98)00177-6.
Burdige, D.J., 2007. Preservation of organic matter in marine sediments: controls, mechanisms, and an imbalance in sediment organic carbon budgets? Chem. Rev. 107, 467–485. https://doi.org/10.1021/cr050347q.
Bush, R.T., McInerney, F.A., 2013. Leaf wax *n*-alkane distributions in and across modern plants: implications for paleoecology and chemotaxonomy. Geochem. Cosmochim. Acta 117, 161–179. https://doi.org/10.1016/j.gca.2013.04.016.
Canuel, E.A., Martens, C.S., 1996. Reactivity of recently deposited organic matter: degradation of lipid compounds near the sediment-water interface. Geochem. Cosmochim. Acta 60, 1793–1806. https://doi.org/10.1016/0016-7037(96)00045-2.
Chagué, C., 2020. Applications of geochemical proxies in paleotsunami research. In: Engel, M., Pilarczyk, J., May, S.M., Brill, D., Garrett, E. (Eds.), Geological Records of Tsunamis and Other Extreme Waves. Elsevier, Amsterdam, pp. 381–401. https://doi.org/10.1016/B978-0-12-815686-5.00018-3.
Chagué, C., Cope, J., Kilroy, C., Jacobsen, G., Zawadzki, A., Wong, H., 2020. A 7300 year record of environmental changes in a coastal wetland (moawhitu), New Zealand, and evidence for catastrophic overwash (tsunami?). Sediment. Geol. 407, 105746. https://doi.org/10.1016/j.sedgeo.2020.105746.
Chagué, C., Shinozaki, T., 2023. Characteristics of the 2011 muddy and organic-rich tsunami deposits in the Tohoku region: an overview. J. Geogr. 132, 341–352. https://doi.org/10.5026/jgeography.132.341.
Chagué-Goff, C., 2010. Chemical signatures of palaeotsunamis: a forgotten proxy? Mar. Geol. 271, 67–71. https://doi.org/10.1016/j.margeo.2010.01.010.
Chagué-Goff, C., Andrew, A., Szczuciński, W., Goff, J., Nishimura, Y., 2012. Geochemical signatures up to the maximum inundation of the 2011 Tohoku-oki tsunami – implications for the 869 AD Jogan and other palaeotsunamis. Sed. Geol. 282, 65–77. https://doi.org/10.1016/j.sedgeo.2012.05.021.
Chagué-Goff, C., Goff, J., Wong, H.K., Cisternas, M., 2015. Insights from geochemistry and diatoms to characterise a tsunami's deposit and maximum inundation limit. Mar. Geol. 359, 22–34. https://doi.org/10.1016/j.margeo.2014.11.00.
Chagué-Goff, C., Schneider, J.L., Goff, J.R., Dominey-Howes, D., Strotz, L., 2011. Expanding the proxy toolkit to help identify past events – lessons from the 2004 Indian Ocean Tsunami and the 2009 South Pacific Tsunami. Earth Sci. Rev. 107, 107–122. https://doi.org/10.1016/j.earscirev.2011.03.007.
Chagué-Goff, C., Szczuciński, W., Shinozaki, T., 2017. Applications of geochemistry in tsunami research: a review. Earth Sci. Rev. 165, 203–244. https://doi.org/10.1016/j.earscirev.2016.12.003.
Chetia, R., Mathews, R.P., Singh, P.K., Sharma, A., 2022. Conifer-mixed tropical rainforest in the Indian Paleogene: new evidences from terpenoid signatures. Palaeogeogr. Palaeoclimatol. Palaeoecol. 596, 110980. https://doi.org/10.1016/j.palaeo.2022.110980.
Cranwell, P.A., 1981. Diagenesis of free and bound lipids in terrestrial detritus deposited in a lacustrine sediment. Org. Geochem. 3, 79–89. https://doi.org/10.1016/0146-6380(81)90002-4.
Cranwell, P.A., 1991. Paleolimnological studies using sequential lipid extraction from recent lacustrine sediment: recognition of source organisms from biomarkers. Hydrobiologia 214, 293–303. https://doi.org/10.1007/BF00050963.
Dawson, A.G., Shi, S., 2000. Tsunami deposits. Pure Appl. Geophys. 157, 875–897. https://doi.org/10.1007/s000240050010.
De Leeuw, J.W., Baas, M., 1986. Early-stage diagenesis of steroids. In: Johns, R.B. (Ed.), Biological Markers in the Sedimentary Record. Methods in Geochemistry and Geophysics 24. Elsevier, Amsterdam, pp. 101–123.
Didyk, B.M., Simoneit, B.R.T., Brassell, S.T., Eglinton, G., 1978. Organic geochemical indicators of palaeoenvironmental conditions of sedimentation. Nature 272, 216–222. https://doi.org/10.1038/272216a0.
Diefendorf, A.F., Freeman, K.H., Wing, S.L., 2014. A comparison of terpenoid and leaf fossil vegetation proxies in Paleocene and Eocene Bighorn Basin sediments. Org. Geochem. 71, 30–42. https://doi.org/10.1016/j.orggeochem.2014.04.004.
Diefendorf, A.F., Leslie, A.B., Wing, S.L., 2019. A phylogenetic analysis of conifer diterpenoids and their carbon isotopes for chemotaxonomic applications. Org. Geochem. 127, 50–58. https://doi.org/10.1016/j.orggeochem.2018.11.007.
Doğrul Selver, A., Sparkes, R.B., Bischoff, J., Talbot, H.M., Gustafsson, Ö., Semiletov, I.P., Dudarev, O.V., Boult, S., van Dongen, B.E., 2015. Distributions of bacterial and archaeal membrane lipids in surface sediments reflect differences in input and loss of terrestrial organic carbon along a cross-shelf Arctic transect. Org. Geochem. 83, 16–26. https://doi.org/10.1016/j.orggeochem.2015.01.005.
Eglinton, T.I., Eglinton, G., 2008. Molecular proxies for paleoclimatology. Earth Planet Sci. Lett. 275, 1–16. https://doi.org/10.1016/j.epsl.2008.07.012.
Eglinton, G., Hamilton, R.J., 1967. Leaf epicuticular Waxes: the waxy outer surfaces of most plants display a wide diversity of fine structure and chemical constituents. Science 156, 1322–1335. https://doi.org/10.1126/science.156.3780.1322.
Engel, M., Schön, I., Patel, T., Pawłowski, J., Szczuciński, W., Dawson, S., Garrett, E., Heyvaert, V.M., 2020. Paleogenetic approaches in tsunami deposit studies. In: Engel, M., Pilarczyk, J., May, S.M., Brill, D., Garrett, E. (Eds.), Geological Records of Tsunamis and Other Extreme Waves. Elsevier, Amsterdam, pp. 427–442. https://doi.org/10.1016/B978-0-12-815686-5.00020-1.
Fahlbusch, K.G., Hammerschmidt, F.J., Panten, J., Pickenhagen, W., Schatkowski, D., Bauer, K., Garbe, D., Surburg, H., 2003. Flavors and fragrances. In: Ullmann's Encyclopedia of Industrial Chemistry. Wiley-VCH, Weinheim. https://doi.org/10.1002/14356007.a11_141.
Folk, R.L., Ward, W.C., 1957. Brazos river bar [texas]; a study in the significance of grain size parameters. J. Sediment. Res. 27, 3–26. https://doi.org/10.1306/74D70646-2B21-11D7-8648000102C1865D.
Franke, S., Schwarzbauer, J., Francke, W., 1998. Arylesters of alkylsulfonic acids in sediments part III of organic compounds as contaminants of the elbe river and its tributaries: part III of organic compounds as contaminants of the Elbe river and its tributaries. Fresenius' J. Anal. Chem. 360, 580–588. https://doi.org/10.1007/s002160050762.
Frenken, M., Bellanova, P., Nishimura, Y., Reicherter, K., Schwarzbauer, J., 2022b. Distribution of the geochemical signature caused by the 2011 Tohoku-oki tsunami in misawa harbor, northern Japan. Nat. Hazards 114, 313–333. https://doi.org/10.1007/s11069-022-05391-y.
Frenken, M., Bellanova, P., Nishimura, Y., Schulte, P., Lehmkuhl, F., Reicherter, K., Schwarzbauer, J., 2022a. Suitable indicators to determine tsunami impact on coastal areas in Northern Japan, Aomori prefecture. Environ. Monit. Assess. 194, 385. https://doi.org/10.1007/s10661-022-09989-4.
Gaffney, V., Fitch, S., Bates, M., Ware, R.L., Kinnaird, T., Gearey, B., Hill, T., Telford, R., Batt, C., Stern, B., Whittakter, J., Davies, S., Sharada, M.B., Everett, R., Cribdon, R., Kistler, L., Harris, S., Kearney, K., Walker, J., Muru, M., Allaby, R.G., 2020. Multi-proxy characterisation of the Storegga tsunami and its impact on the early Holocene landscapes of the southern North sea. Geosci. 10, 270. https://doi.org/10.3390/geosciences10070270.
Gardade, L., Khandeparker, L., Desai, D.V., Atchuthan, P., Anil, A.C., 2021. Fatty acids as indicators of sediment organic matter dynamics in a monsoon-influenced tropical Estuary. Ecol. Indic. 130, 108014. https://doi.org/10.1016/j.ecolind.2021.108014.
Garrett, E., Fujiwara, O., Riedesel, S., Walstra, J., Deforce, K., Yokoyama, Y., Schmidt, S., Brückner, H., De Batist, M., Heyvaert, V.M.A., QuakeRecNankai Team, 2018. Historical Nankai-Suruga megathrust earthquakes recorded by tsunami and terrestrial mass movement deposits on the Shirasuka coastal lowlands, Shizuoka Prefecture, Japan. Holocene 28, 968–983. https://doi.org/10.1177/0959683617752844.
Gee, G.W., Or, D., 2002. Particle-size analysis. In: Dane, J.H., Topp, G.C. (Eds.), Methods of Soil Analysis: Part, 4. Physical Methods. Soil Science Society of America, Madison, WI, pp. 255–293. https://doi.org/10.2136/sssabookser5.4.c12.
Geospatial Information Authority of Japan, 2025. Natural Disaster Memorial Monument. https://www.gsi.go.jp/bousaichiri/denshouhi.html. (Accessed 31 October 2025) *(in Japanese)*.
Goff, J., Chagué-Goff, C., Nichol, S., Jaffe, B., Dominey-Howes, D., 2012. Progress in palaeotsunami research. Sediment. Geol. 243, 70–88. https://doi.org/10.1016/j.sedgeo.2011.11.002.
Gonçalves, F.T., 2002. Organic and isotope geochemistry of the Early Cretaceous rift sequence in the camamu basin, Brazil: paleolimnological inferences and source rock models. Org. Geochem. 33, 67–80. https://doi.org/10.1016/S0146-6380(01)00128-0.
Goodwin, T.W., Mercer, E.I., 1983. Introduction to Plant Biochemistry, second ed. Pergamon Press.
Goossens, H.D., De Leeuw, J.W., Schenck, P.A., Brassell, S.C., 1984. Tocopherols as likely precursors of pristane in ancient sediments and crude oils. Nature 312, 440–442. https://doi.org/10.1038/312440a0.
Goto, K., Chagué-Goff, C., Fujino, S., Goff, J., Jaffe, B., Nishimura, Y., Richmond, B., Sugawara, D., Szczuciński, W., Tappin, D.R., Witter, R.C., Yulianto, E., 2011. New insights of tsunami hazard from the 2011 Tohoku-oki event. Mar. Geol. 290, 46–50. https://doi.org/10.1016/j.margeo.2011.10.004.
Goto, K., Hashimoto, K., Sugawara, D., Yanagisawa, H., Abe, T., 2014. Spatial thickness variability of the 2011 Tohoku-oki tsunami deposits along the coastline of Sendai Bay. Mar. Geol. 358, 38–48. https://doi.org/10.1016/j.margeo.2013.12.015.
Goto, K., Ishizawa, T., Ebina, Y., Imamura, F., Sato, S., Udo, K., 2021. Ten years after the 2011 Tohoku-oki earthquake and tsunami: geological and environmental effects and implications for disaster policy changes. Earth Sci. Rev. 212, 103417. https://doi.org/10.1016/j.earscirev.2020.103417.
Goto, T., Satake, K., Sugai, T., Ishibe, T., Harada, T., Gusman, A.R., 2019. Tsunami history over the past 2000 years on the Sanriku coast, Japan, determined using gravel deposits to estimate tsunami inundation behavior. Sediment. Geol. 382, 85–102. https://doi.org/10.1016/j.sedgeo.2019.01.001.

Goto, T., Satake, K., Sugai, T., Ishibe, T., Harada, T., Murotani, S., 2015. Historical tsunami and storm deposits during the last five centuries on the Sanriku coast, Japan. Mar. Geol. 367, 105–117. https://doi.org/10.1016/j.margeo.2015.05.009.

Hatori, T., 2009. Regional deviation of inundation heights due to the large Sanriku tsunamis. Historical Earthquake (Rekishi Jishin) 24, 41–48 (in Japanese).

Hautevelle, Y., Michels, R., Malartre, F., Trouiller, A., 2006. Vascular plant biomarkers as proxies for palaeoflora and palaeoclimatic changes at the Dogger/Malm transition of the paris basin (France). Org. Geochem. 37, 610–625. https://doi.org/10.1016/j.orggeochem.2005.12.010.

Hawkes, A.D., 2020. Foraminifera in tsunami deposits. In: Engel, M., Pilarczyk, J., May, S.M., Brill, D., Garrett, E. (Eds.), Geological Records of Tsunamis and Other Extreme Waves. Elsevier, Amsterdam, pp. 239–259. https://doi.org/10.1016/B978-0-12-815686-5.00012-2.

Hiraoka, S., Machiyama, A., Ijichi, M., Inoue, K., Oshima, K., Hattori, M., Yoshizawa, S., Kogure, K., Iwasaki, W., 2016. Genomic and metagenomic analysis of microbes in a soil environment affected by the 2011 great East Japan earthquake tsunami. BMC Genom. 17, 53. https://doi.org/10.1186/s12864-016-2380-4.

Hirave, P., Wiesenberg, G.L.B., Birkholz, A., Alewell, C., 2020. Understanding the effects of early degradation on isotopic tracers for CSIA-based sediment source attribution. Biogeosciences 17, 2169–2186. https://doi.org/10.5194/bg-17-2169-2020.

Hopmans, E.C., Weijers, J.W.H., Schefuß, E., Herfort, L., Sinninghe Damsté, J.S., Schouten, S., 2004. A novel proxy for terrestrial organic matter in sediments based on branched and isoprenoid tetraether lipids. Earth Planet Sci. Lett. 224, 107–116. https://doi.org/10.1016/j.epsl.2004.05.012.

Huang, W.Y., Meinschein, W.G., 1979. Sterols as ecological indicators. Geochem. Cosmochim. Acta 43, 739–745. https://doi.org/10.1016/0016-7037(79)90257-6.

Hudson, E.D., Parrish, C.C., Helleur, R.J., 2001. Biogeochemistry of sterols in plankton, settling particles and recent sediments in a cold ocean ecosystem (Trinity Bay, Newfoundland). Mar. Chem. 76, 253–270. https://doi.org/10.1016/S0304-4203(01)00066-4.

Hunt, J.M., 1996. Petroleum Geochemistry and Geology, second ed. W.H. Freeman, New York.

Ikehara, K., Irino, T., Saito, Y., 2021. The 2011 Tohoku-oki tsunami-induced sediment remobilization on the Sendai shelf, Japan, from a comparison of pre-and post-tsunami surface sediments. Sci. Rep. 11, 7864. https://doi.org/10.1038/s41598-021-87152-8.

Inoue, T., Goto, K., Nishimura, Y., Watanabe, M., Iijima, Y., Sugawara, D., 2017. Paleo-tsunami history along the northern Japan trench: evidence from Noda village, northern sanriku coast, Japan. Prog. Earth Planet. Sci. 4, 1–15. https://doi.org/10.1186/s40645-017-0158-1.

Ishimura, D., 2017. Re-examination of the age of historical and paleo-tsunami deposits at Koyadori on the Sanriku Coast, Northeast Japan. Geosci. Lett. 4, 1–12. https://doi.org/10.1186/s40562-017-0077-4.

Ishimura, D., Miyauchi, T., 2015. Historical and paleo-tsunami deposits during the last 4000 years and their correlations with historical tsunami events in Koyadori on the Sanriku Coast, northeastern Japan. Prog. Earth Planet. Sci. 2, 1–18. https://doi.org/10.1186/s40645-015-0047-4.

Ishimura, D., Miyauchi, T., 2017. Holocene environmental changes and paleo-tsunami history in onuma on the southern part of the Sanriku Coast, northeast Japan. Mar. Geol. 386, 126–139. https://doi.org/10.1016/j.margeo.2017.01.011.

Ishizawa, T., Goto, K., Nishimura, Y., Miyairi, Y., Sawada, C., Yokoyama, Y., 2022. Paleotsunami history along the northern Japan trench based on sequential dating of the continuous geological record potentially inundated only by large tsunamis. Quat. Sci. Rev. 279, 107381. https://doi.org/10.1016/j.quascirev.2022.107381.

Jagodziński, R., Sternal, B., Szczuciński, W., Chagué-Goff, C., Sugawara, D., 2012. Heavy minerals in the 2011 Tohoku-oki tsunami deposits – insights into sediment sources and hydrodynamics. Sediment. Geol. 282, 57–64. https://doi.org/10.1016/j.sedgeo.2012.07.015.

Jetter, R., Kunst, L., Samuels, A.L., 2006. Composition of plant cuticular waxes. In: Riederer, M., Müller, C. (Eds.), Biology of the Plant Cuticle (Annual Plant Reviews, 23. Blackwell, Oxford, pp. 145–181. https://doi.org/10.1002/9780470988718.ch4.

Jones, D.M., Rowland, S.J., Douglas, A.G., 1986. Steranes as indicators of petroleum-like hydrocarbons in marine surface sediments. Mar. Pollut. Bull. 17, 24–27. https://doi.org/10.1016/0025-326X(86)90800-3.

Judd, K., Chagué-Goff, C., Goff, J., Gadd, P., Zawadzki, A., Fierro, D., 2017. Multi-proxy evidence for small historical tsunamis leaving little or no sedimentary record. Mar. Geol. 385, 204–215. https://doi.org/10.1016/j.margeo.2017.01.002.

Kanamori, H., 1971. Seismological evidence for a lithospheric normal faulting – the Sanriku earthquake of 1933. Phys. Earth Planet. Inter. 4, 289–300. https://doi.org/10.1016/0031-9201(71)90013-6.

Keeling, C.I., Bohlmann, J., 2006. Genes, enzymes and chemicals of terpenoid diversity in the constitutive and induced defence of conifers against insects and pathogens. New Phytol. 170, 657–675. https://doi.org/10.1111/j.1469-8137.2006.01716.x.

Keil, R.G., Hedges, J.I., 1993. Sorption of organic matter to mineral surfaces and the preservation of organic matter in coastal marine sediments. Chem. Geol. 107, 385–388. https://doi.org/10.1016/0009-2541(93)90215-5.

Kesselmeier, J., Staudt, M., 1999. Biogenic volatile organic compounds (VOC): an overview on emission, physiology and ecology. J. Atmos. Chem. 33, 23–88. https://doi.org/10.1023/A:1006127516791.

Killops, S.D., Killops, V.J., 2013. Introduction to Organic Geochemistry, second ed. Wiley-Blackwell, Hoboken, NJ. https://doi.org/10.1002/9781118697214.

Komeiji, K., Shinozaki, T., Sugawara, D., Ishizawa, T., Ikehara, M., Fujino, S., 2025. High-precision estimation of a paleo-tsunami inundation area by identifying tsunami traces beyond sandy tsunami deposits: a case study of the 869 CE Jogan tsunami in Fukushima, northeastern Japan. Mar. Geol. 481, 107490. https://doi.org/10.1016/j.margeo.2025.107490.

Konechnaya, O., Bellanova, P., Frenken, M., Reicherter, K., Schwarzbauer, J., 2022. Evaluation of organic indicators derived from extractable, hydrolysable and macromolecular organic matter in sedimentary tsunami deposits. Mar. Geol. 443, 106671. https://doi.org/10.1016/j.margeo.2021.106671.

Kortekaas, S., Dawson, A.G., 2007. Distinguishing tsunami and storm deposits: an example from Martinhal, SW Portugal. Sediment. Geol. 200, 208–221. https://doi.org/10.1016/j.sedgeo.2007.01.004.

Marchand, D., Rontani, J.F., 2001. Characterisation of photo-oxidation and autoxidation products of phytoplanktonic monounsaturated fatty acids in marine particulate matter and recent sediments. Org. Geochem. 32, 287–304. https://doi.org/10.1016/S0146-6380(00)00175-3.

Marmulla, R., Harder, J., 2014. Microbial monoterpene transformations – a review. Front. Microbiol. 5, 346. https://doi.org/10.3389/fmicb.2014.00346.

Maruoka, N., Okubo, M., Shibata, H., Gao, X., Ito, T., Kitamura, S.Y., 2015. Improvement of desalted paddy soil by the application of fertilizer made of steelmaking slag (recovery of a paddy field damaged by the tsunami using fertilizer made of steelmaking Slag-1). Tetsu-To-Hagane 101, 445–456. https://doi.org/10.2355/tetsutohagane.TETSU-2014-131.

Marzi, R., Torkelson, B.E., Olson, R.K., 1993. A revised carbon preference index. Org. Geochem. 20, 1303–1306. https://doi.org/10.1016/0146-6380(93)90016-5.

Mathes-Schmidt, M., Schwarzbauer, J., Papanikolaou, I., Syberberg, F., Thiele, A., Wittkopp, F., Reicherter, K., 2013. Geochemical and micropaleontological investigations of tsunamigenic layers along the Thracian Coast (Northern Aegean sea, Greece). Z. f. Geomorphol 57, 5–27. https://doi.org/10.1127/0372-8854/2013/S-00153.

Meyers, P.A., 1997. Organic geochemical proxies of paleoceanographic, paleolimnologic, and paleoclimatic processes. Org. Geochem. 27, 213–250. https://doi.org/10.1016/S0146-6380(97)00049-1.

Meyers, P.A., 2003. Applications of organic geochemistry to paleolimnological reconstructions: a summary of examples from the laurentian Great Lakes. Org. Geochem. 34, 261–289. https://doi.org/10.1016/S0146-6380(02)00168-7.

Meyers, P.A., Ishiwatari, R., 1993. Lacustrine organic geochemistry – an overview of indicators of organic matter sources and diagenesis in lake sediments. Org. Geochem. 20, 867–900. https://doi.org/10.1016/0146-6380(93)90100-P.

Minoura, K., Imamura, F., Sugawara, D., Kono, Y., Iwashita, T., 2001. The 869 Jogan tsunami deposit and recurrence interval of large-scale tsunami on the Pacific coast of northeast Japan. J. Nat. Disaster Sci. 23, 83–88.

Minoura, K., Nakaya, S., 1991. Traces of tsunami preserved in inter-tidal lacustrine and marsh deposits: some examples from northeast Japan. J. Geol. 99, 265–287. https://doi.org/10.1086/629488.

Mizukawa, K., Hirai, Y., Sakakibara, H., Endo, S., Okuda, K., Takada, H., Murakami-Sugihara, N., Shirai, K., Ogawa, H., 2017. Spatial distribution and temporal trend of anthropogenic organic compounds derived from the 2011 East Japan Earthquake. Arch. Environ. Contam. Toxicol. 73, 185–195. https://doi.org/10.1007/s00244-017-0389-6.

Moreira, S., Costa, P.J.M., Andrade, C., Ponte Lira, C., Freitas, M.C., Oliveira, M.A., Reichart, G.-J., 2017. High resolution geochemical and grain-size analysis of the AD 1755 tsunami deposit: insights into the inland extent and inundation phases. Mar. Geol. 390, 94–105. https://doi.org/10.1016/j.margeo.2017.04.007.

Morton, R.A., Gelfenbaum, G., Jaffe, B.E., 2007. Physical criteria for distinguishing sandy tsunami and storm deposits using modern examples. Sediment. Geol. 200, 184–207. https://doi.org/10.1016/j.sedgeo.2007.01.003.

Morton, R.A., Sallenger Jr, A.H., 2003. Morphological impacts of extreme storms on sandy beaches and barriers. J. Coast Res. 19, 560–573. https://www.jstor.org/stable/4299198.

Nakata, T., Shimazaki, K., 1997. Geo-slicer, a newly invented soil sampler, for high-resolution active fault studies. J. Geogr. 106, 59–69 (in Japanese).

Namegaya, Y., Satake, K., Yamaki, S., 2010. Numerical simulation of the AD 869 Jōgan tsunami in Ishinomaki and Sendai plains and Ukedo river-mouth lowland. Annu. Rep. Active Fault Paleoearthq. Res. 10, 1–21 (in Japanese).

Namegaya, Y., Satake, K., 2014. Reexamination of the A.D. 869 Jōgan earthquake size from tsunami deposit distribution, simulated flow depth, and velocity. Geophys. Res. Lett. 41, 2297–2303. https://doi.org/10.1002/2013GL058678.

Naruse, H., Arai, K., Matusmoto, D., Takahashi, H., Yamashita, S., Tanaka, G., Murayama, M., 2012. Sedimentary features observed in the tsunami deposits at Rikuzentakata City, northeastern Japan. Sediment. Geol. 282, 40–56. https://doi.org/10.1016/j.sedgeo.2012.08.012.

Ünlü, S., Alpar, B., Altınok, Y., Özer, N., 2012. Rapid coastal changes and tsunami impacts at the Patara Harbour (Turkey). In: Proceedings of the International Conference on Land–Sea Interactions in the Coastal Zone (LANDSI 2012). Jounieh, Lebanon, pp. 411–418.

Oppenheimer, C., Wacker, L., Xu, J., Galván, J.D., Stoffel, M., Guillet, S., Corona, C., Sigl, M., Di Cosmo, N., Hajdas, I., Pan, B., Breuker, R., Schneider, L., Esper, J., Fei, J., Hammond, J.O.S., Büntgen, U., 2017. Multi-proxy dating the 'millennium eruption'of Changbaishan to late 946 CE. Quat. Sci. Rev. 158, 164–171. https://doi.org/10.1016/j.quascirev.2016.12.024.

Otto, A., Wilde, V., 2001. Sesqui-, di-, and triterpenoids as chemosystematic markers in extant conifers – a review. Bot. Rev. 67, 141–238. https://doi.org/10.1007/BF02858076.

Ourisson, G., Rohmer, M., Poralla, K., 1987. Prokaryotic hopanoids and other polyterpenoid sterol surrogates. Annu. Rev. Microbiol. 41, 301–333. https://doi.org/10.1146/annurev.mi.41.100187.001505.

Ozawa, S., Nishimura, T., Suito, H., Kobayashi, T., Tobita, M., Imakiire, T., 2011. Coseismic and postseismic slip of the 2011 magnitude-9 Tohoku-Oki earthquake. Nature 475, 373–376. https://doi.org/10.1038/nature10227.

Perry, G.J., Volkman, J.K., Johns, R.B., Bavor Jr., H.J., 1979. Fatty acids of bacterial origin in contemporary marine sediments. Geochem. Cosmochim. Acta 43, 1715–1725. https://doi.org/10.1016/0016-7037(79)90020-6.
Peters, K.E., Walters, C.C., Moldowan, J.M., 2005. The biomarker guide In: Biomarkers and Isotopes in the Environment and Human History, second ed., 1. Cambridge University Press, Cambridge. https://doi.org/10.1017/CBO9780511524868.
Peters, R., Jaffe, B., 2010. Identification of tsunami deposits in the geologic record; developing criteria using recent tsunami deposits. In: U.S. Geological Survey Open-File Report 2010–1239, iv, p. 28. https://doi.org/10.3133/ofr20101239.
Peters, K.E., Moldowan, J.M., 1991. Effects of source, thermal maturity, and biodegradation on the distribution and isomerization of homohopanes in petroleum. Org. Geochem. 17, 47–61. https://doi.org/10.1016/0146-6380(91)90039-M.
Peters, K.E., Moldowan, J.M., 1993. The Biomarker Guide: Interpreting Molecular Fossils in Petroleum and Ancient Sediments. Prentice Hall, Englewood Cliffs, NJ.
Pilarczyk, J.E., Horton, B.P., Witter, R.C., Vane, C.H., Chagué-Goff, C., Goff, J., 2012. Sedimentary and foraminiferal evidence of the 2011 Tōhoku-oki tsunami on the Sendai coastal plain, Japan. Sed. Geol. 282, 78–89. https://doi.org/10.1016/j.sedgeo.2012.08.011.
Powell, T.G., 1988. Pristane/phytane ratio as environmental indicator. Nature 333, 604. https://doi.org/10.1038/333604a0, 604.
Prahl, F.G., Pinto, L.A., 1987. A geochemical study of long-chain n-aldehydes in Washington coastal sediments. Geochem. Cosmochim. Acta 51, 1573–1582. https://doi.org/10.1016/0016-7037(87)90338-3.
Putra, P.S., Yulianto, E., Nugroho, S.H., 2023. Distribution patterns of Foraminifera in paleotsunami layers: a review. Nat. Haz. Res. 3, 1–13. https://doi.org/10.1016/j.nhres.2022.12.004.
Rabbani, A.R., Kamali, M.R., 2005. Source rock evaluation and petroleum geochemistry, offshore SW Iran. J. Petrol. Geol. 28, 413–428. https://doi.org/10.1111/j.1747-5457.2005.tb00091.x.
Richmond, B., Szczuciński, W., Chagué-Goff, C., Goto, K., Sugawara, D., Witter, R., Tappin, D.R., Jaffe, B., Fujino, S., Nishimura, Y., Goff, J., 2012. Erosion, deposition and landscape change on the Sendai coastal plain, Japan, resulting from the March 11, 2011 Tohoku-oki tsunami. Sediment. Geol. 282, 27–39. https://doi.org/10.1016/j.sedgeo.2012.08.005.
Rohmer, M., Bouvier-Navé, P., Ourisson, G., 1984. Distribution of hopanoid triterpenes in prokaryotes. J. Gen. Microbiol. 130, 1137–1150. https://doi.org/10.1099/00221287-130-5-1137.
Rontani, J.F., 2001. Visible light-dependent degradation of lipidic phytoplanktonic components during senescence: a review. Phytochemistry 58, 187–202. https://doi.org/10.1016/S0031-9422(01)00202-3.
Rontani, J.F., Jameson, I., Christodoulou, S., Volkman, J.K., 2007. Free radical oxidation (autoxidation) of alkenones and other lipids in cells of Emiliania huxleyi. Phytochemistry 68, 913–924. https://doi.org/10.1016/j.phytochem.2006.12.013.
Rontani, J.F., Volkman, J.K., Prahl, F.G., Wakeham, S.G., 2013. Biotic and abiotic degradation of alkenones and implications for U37K′ paleoproxy applications: a review. Org. Geochem. 59, 95–113. https://doi.org/10.1016/j.orggeochem.2013.04.005.
Rontani, J.F., Bonin, P., 2011. Production of pristane and phytane in the marine environment: role of prokaryotes. Res. Microbiol. 162, 923–933. https://doi.org/10.1016/j.resmic.2011.01.012.
Rontani, J.F., Volkman, J.K., 2003. Phytol degradation products as biogeochemical tracers in aquatic environments. Org. Geochem. 34, 1–35. https://doi.org/10.1016/S0146-6380(02)00185-7.
Satake, K., 2008. Numerical simulation of the AD 869 Jogan tsunami in Ishinomaki and Sendai plains. Annu. Rep. Active Fault Paleoearthq. Res. 8, 71–89 (in Japanese).
Satake, K., Fujii, Y., Yamaki, S., 2017. Different depths of near-trench slips of the 1896 Sanriku and 2011 Tohoku earthquakes. Geosci. Lett. 4, 33. https://doi.org/10.1186/s40562-017-0099-y.
Sawai, Y., 2007. A study on paleotsunami using handy geoslicer in Sendai plain (Sendai, Natori, iwanuma, Watari, and Yamamoto), Miyagi, Japan. Annu. Rep. Active fault paleoarthq. Res. 7, 47–80 (in Japanese).
Sawai, Y., Fujii, Y., Fujiwara, O., Kamataki, T., Komatsubara, J., Okamura, Y., Satake, K., Shishikura, M., 2008. Marine incursions of the past 1500 years and evidence of tsunamis at Suijin-numa, a coastal lake facing the Japan Trench. Holocene 18, 517–528. https://doi.org/10.1177/09596836080892.
Sawai, Y., Namegaya, Y., Okamura, Y., Satake, K., Shishikura, M., 2012. Challenges of anticipating the 2011 Tohoku earthquake and tsunami using coastal geology. Geophys. Res. Lett. 39. https://doi.org/10.1029/2012GL053692.
Sawai, Y., Namegaya, Y., Tamura, T., Nakashima, R., Tanigawa, K., 2015. Shorter intervals between great earthquakes near Sendai: scour ponds and a sand layer attributable to AD 1454 overwash. Geophys. Res. Lett. 42, 4795–4800. https://doi.org/10.1002/2015GL064167.
Scalan, E.S., Smith, J.E., 1970. An improved measure of the odd-even predominance in the normal alkanes of sediment extracts and petroleum. Geochem. Cosmochim. Acta 34, 611–620. https://doi.org/10.1016/0016-7037(70)90019-0.
Schouten, S., Hopmans, E.C., Sinninghe Damsté, J.S., 2013. The organic geochemistry of glycerol dialkyl glycerol tetraether lipids: a review. Org. Geochem. 54, 19–61. https://doi.org/10.1016/j.orggeochem.2012.09.006.
Schwarzbauer, J., Littke, R., Weigelt, V., 2000. Identification of specific organic contaminants for estimating the contribution of the Elbe river to the pollution of the German bight. Org. Geochem. 31, 1713–1731. https://doi.org/10.1016/S0146-6380(00)00076-0.
Seifert, W.K., Moldowan, J.M., 1986. Use of biological markers in petroleum exploration. In: Johns, R.B. (Ed.), Biological Markers in the Sedimentary Record. Methods in Geochemistry and Geophysics, 24. Elsevier, Amsterdam, pp. 261–290.
Sepúlveda, J., Wendler, J., Leider, A., Kuss, H.J., Summons, R.E., Hinrichs, K.U., 2009. Molecular isotopic evidence of environmental and ecological changes across the Cenomanian–Turonian boundary in the levant platform of central Jordan. Org. Geochem. 40, 553–568. https://doi.org/10.1016/j.orggeochem.2009.02.009.
Shanmugam, G., 1985. Significance of coniferous rain forests and related organic matter in generating commercial quantities of oil, gippsland Basin, Australia. AAPG (Am. Assoc. Pet. Geol.) Bull. 69 (8), 1241–1254. https://doi.org/10.1306/AD462BC3-16F7-11D7-8645000102C1865D.
Shinozaki, T., 2021. Geochemical approaches in tsunami research: current knowledge and challenges. Geosci. Lett 8. https://doi.org/10.1186/s40562-021-00177-9.
Shinozaki, T., Fujino, S., Ikehara, M., Sawai, Y., Tamura, T., Goto, K., Sugawara, D., Abe, T., 2015. Marine biomarkers deposited on coastal land by the 2011 Tohoku-oki tsunami. Nat. Hazards 77, 445–460. https://doi.org/10.1007/s11069-015-1598-9.
Shinozaki, T., Iguchi, A., Nishijima, M., Goto, K., Fujino, S., 2025. Identification of deposits from modern and ancient large tsunamis by means of environmental DNA. Sci. Rep. 15, 242. https://doi.org/10.1038/s41598-024-84245-y.
Shinozaki, T., Sawai, Y., Hara, J., Ikehara, M., Matsumoto, D., Tanigawa, K., 2016. Geochemical characteristics of deposits from the 2011 Tohoku-oki tsunami at hasunuma, Kujukuri coastal plain. Japan. Isl. Arc 25, 350–368. https://doi.org/10.1111/iar.12159.
Shinozaki, T., Sawai, Y., Ikehara, M., Matsumoto, D., Shimada, Y., Tanigawa, K., Tamura, T., 2022. Identifying tsunami traces beyond sandy tsunami deposits using terrigenous biomarkers: a case study of the 2011 Tohoku-oki tsunami in a coastal pine forest, northern Japan. Prog. Earth Planet. Sci. 9, 1–10. https://doi.org/10.1186/s40645-022-00491-6.
Shishikura, M., 2007. Age and distribution of tsunami deposit in the Ishinomaki plain, northeast Japan. Annu. Rep. Active Fault Paleoearthq. Res. 7, 31–46 (in Japanese).
Shunthirasingham, C., Simpson, M.J., 2006. Investigation of bacterial hopanoid inputs to soils from Western Canada. Appl. Geochem. 21, 964–976. https://doi.org/10.1016/j.apgeochem.2006.03.007.
Sinninghe Damsté, J.S., Van Duin, A.C., Hollander, D., Kohnen, M.E., De Leeuw, J.W., 1995. Early diagenesis of bacteriohopanepolyol derivatives: formation of fossil homohopanoids. Geochem. Cosmochim. Acta 59, 5141–5157. https://doi.org/10.1016/0016-7037(95)00338-X.
Somboonna, N., Wilantho, A., Jankaew, K., Assawamakin, A., Sangsrakru, D., Tangphatsornruang, S., Tongsima, S., 2014. Microbial ecology of Thailand tsunami and non-tsunami affected terrestrials. PLoS One 9, e94236. https://doi.org/10.1371/journal.pone.0094236.
Spiske, M., Piepenbreier, J., Benavente, C., Bahlburg, H., 2013. Preservation potential of tsunami deposits on arid siliciclastic coasts. Earth Sci. Rev. 126, 58–73. https://doi.org/10.1016/j.earscirev.2013.07.009.
Spiske, M., Tang, H., Bahlburg, H., 2020. Post-depositional alteration of onshore tsunami deposits–implications for the reconstruction of past events. Earth Sci. Rev. 202, 103068. https://doi.org/10.1016/j.earscirev.2019.103068.
Stephanou, E., 1989. Long-chain n-aldehydes: an overlooked but ubiquitous compound class of possible geochemical and environmental significance. Naturwissenschaften 76, 464–467. https://doi.org/10.1007/BF00366223.
Sugawara, D., 2021. Numerical modeling of tsunami: advances and future challenges after the 2011 Tohoku earthquake and tsunami. Earth Sci. Rev. 214, 103498. https://doi.org/10.1016/j.earscirev.2020.103498.
Sugawara, D., Goto, K., Imamura, F., Matsumoto, H., Minoura, K., 2012. Assessing the magnitude of the 869 Jogan tsunami using sedimentary deposits: prediction and consequence of the 2011 Tohoku-oki tsunami. Sediment. Geol. 282, 14–26. https://doi.org/10.1016/j.sedgeo.2012.08.001.
Sugawara, D., Imamura, F., Goto, K., Matsumoto, H., Minoura, K., 2013. The 2011 Tohoku-oki earthquake tsunami: similarities and differences to the 869 Jogan tsunami on the Sendai plain. Pure Appl. Geophys. 170, 831–843. https://doi.org/10.1007/s00024-012-0460-1.
Sugawara, D., Minoura, K., Imamura, F., 2001. Sedimentation due to the A.D. 869 Jōgan tsunami and its numerical reconstruction. Tsunami Engineering Research Report 18, 1–10 (in Japanese).
Suneel, V., Vethamony, P., Naik, B.G., Vinod Kumar, K., Sreenu, L., Samiksha, S.V., Tai, Y., Sudheesh, K., 2014. Source investigation of the tar balls deposited along the Gujarat coast, India, using chemical fingerprinting and transport modeling techniques. Environ. Sci. Technol. 48, 11343–11351. https://doi.org/10.1021/es5032213.
Suppasri, A., Latcharote, P., Bricker, J.D., Leelawat, N., Hayashi, A., Yamashita, K., Makinoshima, F., Roeber, V., Imamura, F., 2016. Improvement of tsunami countermeasures based on lessons from the 2011 great East Japan earthquake and Tsunami – situation after five years. Coast. Eng. J. 58, 1–30. https://doi.org/10.1142/S0578563416400118.
Switzer, A., Yap, W., Lauro, F., Gouramanis, C., Dominey-Howes, D., Labbate, M., 2016. A geomicrobiological approach to differentiate storm and tsunami deposits in the recent geological record. AGU Fall Meeting Abstracts 2016. NH52A-02.
Szczuciński, W., 2020. Post-depositional changes to tsunami deposits and their preservation potential. In: Engel, M., Pilarczyk, J., May, S.M., Brill, D., Garrett, E. (Eds.), Geological Records of Tsunamis and Other Extreme Waves. Elsevier, Amsterdam, pp. 443–469. https://doi.org/10.1016/B978-0-12-815686-5.00021-3.
Szczuciński, W., Kokociński, M., Rzeszewski, M., Chagué-Goff, C., Cachão, M., Goto, K., Sugawara, D., 2012. Sediment sources and sedimentation processes of 2011 Tohoku-oki tsunami deposits on the Sendai Plain, Japan – insights from diatoms, nannoliths and grain size distribution. Sediment. Geol. 282, 40–56. https://doi.org/10.1016/j.sedgeo.2012.07.019.
Szczuciński, W., Pawłowska, J., Lejzerowicz, F., Nishimura, Y., Kokociński, M., Majewski, W., Nakamura, Y., Pawlowski, J., 2016. Ancient sedimentary DNA reveals

past tsunami deposits. Mar. Geol. 381, 29–33. https://doi.org/10.1016/j.margeo.2016.08.006.

Takada, K., Nakata, T., Miyagi, T., Haraguchi, T., Nishitani, Y., 2002. Handy geoslicer – new soil sampler for Quaternary geologist. Chisitsu News 579, 12–18 (in Japanese).

Takada, K., Shishikura, M., Imai, K., Ebina, Y., Goto, K., Koshiya, S., Yamamoto, H., Igarashi, A., Ichihara, T., Kinoshita, H., Ikeda, T., 2016. Distribution and ages of tsunami deposits along the Pacific Coast of the Iwate prefecture. Annu. Rep. Active Fault Paleoearthq. Res. 16, 1–52 (in Japanese).

Talbot, H.M., Farrimond, P., 2007. Bacterial populations recorded in diverse sedimentary biohopanoid distributions. Org. Geochem. 38, 1212–1225. https://doi.org/10.1016/j.orggeochem.2007.04.006.

Tanioka, Y., Satake, K., 1996. Tsunami generation by horizontal displacement of ocean bottom. Geophys. Res. Lett. 23, 861–864. https://doi.org/10.1029/96GL00736.

Taylor, K.A., Harvey, H.R., 2011. Bacterial hopanoids as tracers of organic carbon sources and processing across the western Arctic continental shelf. Org. Geochem. 42, 487–497. https://doi.org/10.1016/j.orggeochem.2011.03.012.

ten Haven, H.L., De Leeuw, J.W., Rullkötter, J., Sinninghe Damsté, J.S., 1987. Restricted utility of the pristane/phytane ratio as a palaeoenvironmental indicator. Nature 330, 641–643. https://doi.org/10.1038/330641a0.

ten Haven, H.L., De Leeuw, J.W., Schenck, P.A., 1985. Organic geochemical studies of a Messinian evaporitic basin, northern apennines (Italy) I: hydrocarbon biological markers for a hypersaline environment. Geochem. Cosmochim. Acta 49, 2181–2191. https://doi.org/10.1016/0016-7037(85)90075-4.

ten Haven, H.L., Rullkötter, J., De Leeuw, J.W., Sinninghe Damsté, J.S., 1988. Pristane/phytane ratio as environmental indicator. Nature 333, 604. https://doi.org/10.1038/333604a0, 604.

Tetsuka, H., Goto, K., Ebina, Y., Sugawara, D., Ishizawa, T., 2021. Historical and geological evidence for the seventeenth-century tsunamis along Kuril and Japan trenches: implications for the origin of the AD 1611 Keicho earthquake and tsunami, and for the probable future risk potential. In: Dilek, Y., Ogawa, Y., Okubo, Y. (Eds.), Characterization of Modern and Historical Seismic-Tsunamic Events, and Their Global-Societal Impacts, 501. Geological Society, London, Special Publications, pp. 269–288. https://doi.org/10.1144/SP501-2019-60.

Thomas, C.L., Jansen, B., van Loon, E.E., Wiesenberg, G.L., 2021. Transformation of *n*-alkanes from plant to soil: a review. Soil 7, 785–809. https://doi.org/10.5194/soil-7-785-2021.

van Roon, A., Parsons, J.R., Krap, L., Govers, H.A., 2005b. Fate and transport of monoterpenes through soils. Part II: calculation of the effect of soil temperature, water saturation and organic carbon content. Chemosphere 61, 129–138. https://doi.org/10.1016/j.chemosphere.2005.02.082.

van Roon, A., Parsons, J.R., te Kloeze, A.M., Govers, H.A., 2005a. Fate and transport of monoterpenes through soils. Part I. Prediction of temperature dependent soil fate model input-parameters. Chemosphere 61, 599–609. https://doi.org/10.1016/j.chemosphere.2005.02.081.

Volkman, J., 2003. Sterols in microorganisms. Appl. Microbiol. Biotechnol. 60, 495–506. https://doi.org/10.1007/s00253-002-1172-8.

Volkman, J.K., 1986. A review of sterol markers for marine and terrigenous organic matter. Org. Geochem. 9, 83–99. https://doi.org/10.1016/0146-6380(86)90089-6.

Volkman, J.K., Barrett, S.M., Blackburn, S.I., Mansour, M.P., Sikes, E.L., Gelin, F., 1998. Microalgal biomarkers: a review of recent research developments. Org. Geochem. 29, 1163–1179. https://doi.org/10.1016/S0146-6380(98)00062-X.

Wakeham, S.G., Lee, C., Hedges, J.I., Hernes, P.J., Peterson, M.L., 1997. Molecular indicators of diagenetic status in marine organic matter. Geochem. Cosmochim. Acta 61, 5363–5369. https://doi.org/10.1016/S0016-7037(97)00312-8.

Watanabe, M., Goto, K., Roeber, V., Imamura, F., 2021. Identification of coastal sand deposits from tsunamis and storm waves based on numerical computations. J. Geophys. Res. Earth Surf. 126, e2021JF006092. https://doi.org/10.1029/2021JF006092.

Watanabe, T., Tsuchiya, N., Yamasaki, S.I., Sawai, Y., Hosoda, N., Nara, F.W., Nakamura, T., Komai, T., 2020. A geochemical approach for identifying marine incursions: implications for tsunami geology on the Pacific coast of northeast Japan. Appl. Geochem. 118, 104644. https://doi.org/10.1016/j.apgeochem.2020.104644.

Yamada, M., Fujino, S., Goto, K., 2014. Deposition of sediments of diverse sizes by the 2011 Tohoku-oki tsunami at Miyako City, Japan. Mar. Geol. 358, 67–78. https://doi.org/10.1016/j.margeo.2014.05.019.

Yap, W., Switzer, A.D., Gouramanis, C., Horton, B.P., Marzinelli, E.M., Wijaya, W., Yan, Y.T., Dominey-Howes, D., Labbate, M., Jankaew, K., Lauro, F.M., 2023. Investigating geological records of tsunamis in Western Thailand with environmental DNA. Mar. Geol., 106989 https://doi.org/10.1016/j.margeo.2023.106989.

Yap, W., Switzer, A.D., Gouramanis, C., Marzinelli, E., Wijaya, W., Yan, Y.T., Dominey-Howes, D., Labbate, M., Srinivasalu, S., Jankaew, K., Lauro, F.M., 2021. Environmental DNA signatures distinguish between tsunami and storm deposition in overwash sand. Commun. Earth Environ. 2, 129. https://doi.org/10.1038/s43247-021-00199-3.

Yokoyama, Y., Sakamoto, I., Takashimizu, Y., Shimizu, Y., 2021. Sedimentological characteristics and distribution of shallow-marine tsunami deposits in Hirota Bay, Sanriku Rias, Japan. J. Sedimentol. Soc. Jap. 79, 47–69.